

1 Leg compliance is required to explain the ground reaction
2 force patterns and speed ranges in different gaits

3 Ali Tehrani Safa^{1,a}, Tirthabir Biswas^{2,3,a}, Arun Ramakrishnan⁴, Vikas Bhandawat^{1*}

4 September 7, 2024

5 ^aequal authors

6 ¹School of Biomedical Engineering, Science and Health Systems
7 Drexel University
8 Philadelphia, PA 19104, USA.

9 ²Department of Neurobiology
10 Northwestern University
11 Evanston, IL 60208, USA.

12 ³Janelia Research Campus
13 Howard Hughes Medical Institute
14 Ashburn, VA 20147, USA.

15 ⁴College of Nursing and Health Professionals
16 Drexel University
17 Philadelphia, PA 19104, USA.

18 **Abstract**

19 Two simple models – vaulting over stiff legs and rebounding over compliant legs – are em-
20 ployed to describe the mechanics of legged locomotion. It is agreed that compliant legs are
21 necessary for describing running and that legs are compliant while walking. Despite this agree-
22 ment, stiff legs continue to be employed to model walking. Here, we show that leg compliance
23 is necessary to model walking and, in the process, identify the principles that underpin two
24 important features of legged locomotion: First, at the same speed, step length, and stance du-
25 ration, multiple gaits that differ in the number of leg contraction cycles are possible. Among
26 them, humans and other animals choose a gait with M-shaped vertical ground reaction forces
27 because it is energetically favored. Second, the transition from walking to running occurs be-
28 cause of the inability to redirect the vertical component of the velocity during the double stance
29 phase. Additionally, we also examine the limits of double spring-loaded pendulum (DSLIP) as a
30 quantitative model for locomotion, and conclude that DSLIP is limited as a model for walking.
31 However, insights gleaned from the analytical treatment of DSLIP are general and will inform
32 the construction of more accurate models of walking.

*Author for correspondence - vb468@drexel.edu

33 1 Introduction

34 Understanding the movement of the center of mass (CoM) and the forces exerted on the CoM
35 during locomotion is important because the behavior of the CoM describes the overall interaction
36 between the animal and the environment during locomotion. The CoM movement and the forces
37 exerted on them follow relatively simple patterns conserved across animals, suggesting that the
38 overall animal-substrate interactions and, therefore, the underlying mechanical principles are simple
39 and general (Blickhan, 1989; Geyer et al., 2006). The best example of the generality of mechanical
40 principles is observed during running: Irrespective of the size of the animal, and the number of legs
41 it uses, during running, the CoM reaches its minimum height at mid-stance and the vertical ground
42 reaction force (vGRF) has an inverted “U”-shaped profile with a midstance maximum. This profile
43 is well-explained by the spring-loaded inverted pendulum (SLIP), in which the mass of the animal
44 is concentrated at a point. This point mass is supported by a massless spring (Blickhan, 1989;
45 McMahon and Cheng, 1990; Blickhan and Full, 1993; Ahn et al., 2004; Daley et al., 2007; Nishikawa
46 et al., 2007; Schmitt, 1999). The success of SLIP at modeling running shows that a body supported
47 by a compliant leg is a good model for running – or locomotion at high speeds.

48 Unlike running, it is unclear whether leg compliance is important for walking – the gait used at
49 low speeds. Initially, the inverted pendulum (IP) model, which uses a non-compliant or rigid leg,
50 was used to model walking (Griffin et al., 2004; Usherwood, 2005; Buczek et al., 2006). The IP
51 model successfully models the energetics of walking (Kuo, 2001; Donelan et al., 2002; Kuo, 2002;
52 Kuo et al., 2005) explaining correctly the exchange of kinetic and potential energy during walking:
53 During the first half of the stance phase, the speed of the CoM decreases as the height of the CoM
54 increases. The increase in potential energy is reconverted into kinetic energy during the second half
55 of the stance phase.

56 With modifications, IP can also model the work done during velocity redirection between steps
57 which is important for estimating the energy cost of walking. During human walking, the CoM
58 velocity vector is directed downwards at the end of the step and must be redirected upwards before
59 the next step (Kuo, 2001; Adamczyk and Kuo, 2009; Donelan et al., 2002). In the IP model, velocity
60 redirection occurs instantaneously, therefore, the work performed during the transition cannot be
61 estimated. Regardless, many trends for work done during walking can be explained by distributing
62 the force impulse in IP over a finite period of time; these modifications, however, are entirely *ad hoc*.
63 Another, perhaps more fundamental, limitation of the IP model is that it cannot model the double-
64 humped or M-shaped vertical GRF (vGRF) during walking. This limitation has been addressed
65 in many ways: by modeling non-impulsive impact forces at the beginning and end of each step,
66 and by using a telescoping actuator with bounds on impact forces (Srinivasan and Ruina, 2006;
67 Srinivasan, 2011). However, the model that produces the most naturalistic force profiles assumes
68 a linear relation between force and leg length, implying that a linear spring is likely necessary to
69 model GRF during walking.

70 The limitation of IP model in producing appropriate forces, the fact that although IP correctly
71 predicts the mid-stance maximum in the height of the CoM, the actual CoM height at mid-stance
72 is lower, and the recent realization that legs are compliant during walking (Lee and Farley, 1998;
73 Buczek et al., 2006) led to the development of the double SLIP (DSLIP) model, in which each leg
74 of a biped is modeled as a spring (Figure 1A). DSLIP extends SLIP with a double stance phase
75 during which the CoM is supported by two “springy” legs (Geyer et al., 2006; Rummel et al., 2010).
76 DSLIP can produce the M-shaped GRFs observed during human walking by providing a smooth
77 velocity redirection during the double stance phase. It also produces trajectories with mid-stance
78 heights that are lower than IP and more in accordance with experimental data. While DSLIP is
79 an attractive model, there are several issues regarding DSLIP as a model for locomotion. The first
80 issue is whether DSLIP can explain the choice of gait. Although it is clear that DSLIP is versatile,
81 and all the major gaits observed during bipedal walking can emerge from the DSLIP model (Gan
82 et al., 2018), it is unclear whether the range of speed over which a gait is observed in DSLIP matches

83 the range of speeds observed in animals. In humans, for example, walking is the dominant mode of
84 transport over a large range of speeds and is characterized by an M-shaped vertical ground reaction
85 force (vGRF). DSLIP finds stable gaits with M-shaped GRF for only a limited range of speeds
86 (Geyer et al., 2006; Lipfert et al., 2012). The reasons for this limited range of speed supported by
87 DSLIP are not understood. Similarly, although humans walk over a wide range of speeds, they do
88 transition to faster gaits like running at speeds much lower than arguments involving centrifugal
89 forces and slipping suggests. Thus, evaluating whether the DSLIP model can explain why M-shaped
90 GRFs are prevalent, and what underlies the transition from M-shaped GRFs to other gaits will
91 provide insights into the role of compliance in walking.

92 A second issue is how well DSLIP models the kinematics and mechanics of human walking. This
93 question has not been evaluated rigorously. In studies in which DSLIP is compared to experimental
94 data, it predicts within-step variations in CoM height and ground reaction forces (GRFs) (Lipfert
95 et al., 2012; Hubel and Usherwood, 2015) that are larger than those observed experimentally. A
96 larger issue is how a successful model is defined. Most studies focus on a single aspect of locomotion
97 such as GRFs. Considering GRFs, CoM kinematics, and real non-dimensionalized time (and not
98 normalized time) at the same time is crucial because the CoM height, H , along with the gravitational
99 acceleration constant, $g \approx 9.8 \text{ m/s}^2$, determines the natural timescale of the system $\sqrt{\frac{R_{nat}}{g}}$, where,
100 $R_{nat} \approx H$, is the natural spring length. A successful model must produce realistic GRFs within the
101 constraints of experimentally observed CoM kinematics and stance duration. These three constraints
102 are rarely satisfied (Maus et al., 2010; Lipfert et al., 2012; Maus et al., 2015) simultaneously in most
103 studies of locomotion, leaving the problem under-constrained. A previous study took this approach
104 to model the single support phase of human walking (Antoniak et al., 2019).

105 These issues raise the question of whether adding compliance to the leg is necessary for modeling
106 human walking. In this study, we show that adding leg compliance through the DSLIP model allows
107 the modeling of fundamental features of locomotion, which would not be possible without it. During
108 locomotion, the radial and angular motions of the CoM must be synchronized. Leg compliance
109 provides a natural mechanistic basis for understanding the implications of this synchronization. We
110 show that leg compliance explains the gaits observed at a given speed and how they relate to different
111 oscillatory modes of the spring. We further argue that the *normal* gait with the characteristic “M”-
112 shaped GRF is preferred because it is energetically efficient. We also show that it is difficult to
113 walk using this normal gait at high speeds because achieving the necessary velocity redirection in
114 the vertical direction is difficult. While DSLIP seems particularly limited in its ability to produce
115 M-shaped GRFs, it enabled us to understand the fundamental reason behind why humans (and
116 other animals) transition to faster gaits at size-specific speeds (Froude number $\equiv (\text{speed})^2/gR_{nat}$)
117 that are significantly lower than 1, the approximate transition speed predicted by IP. We argue
118 that once compliance is added, (which is certainly present during walking) speeds at which walking
119 with a normal gait can occur are limited by the inability to perform large velocity redirections.
120 We also show that linear springs are fundamentally limited and cannot support normal walking
121 above a Froude number ~ 0.25 . Our analysis thus strongly suggests that while a spring with a
122 constant stiffness cannot model human walking except for a narrow range of speeds, a compliant leg
123 is necessary to understand fundamental constraints and optimization criteria that describe walking
124 dynamics. Hence, DSLIP is a far superior starting point for more complex locomotion models than
125 without leg compliance.

126 2 Results

127 Throughout the manuscript, we employ the DSLIP model (Figure 1A) in which both legs are modeled
128 as massless springs to gain insight into the role of compliance in walking. Each leg has the same
129 stiffness, K_s , and natural length, R_{nat} . The dynamics of the single stance phase are the same as
130 SLIP; the swing dynamics are not modeled. The single stance phase transitions to a double stance

131 phase when the distance between the CoM and the future footstep equals the spring's natural length,
 132 and we assume that the swing leg has "touched down". The step length, L , between two consecutive
 133 foot positions is another parameter. We will focus on symmetric gaits so that the lift-off of the
 134 receding leg and the touch-down of the leading leg occur at time points given by time-reversal
 135 symmetry about the mid-step time. All variables in their dimensional and dimensionless forms are
 136 enumerated in the table below.

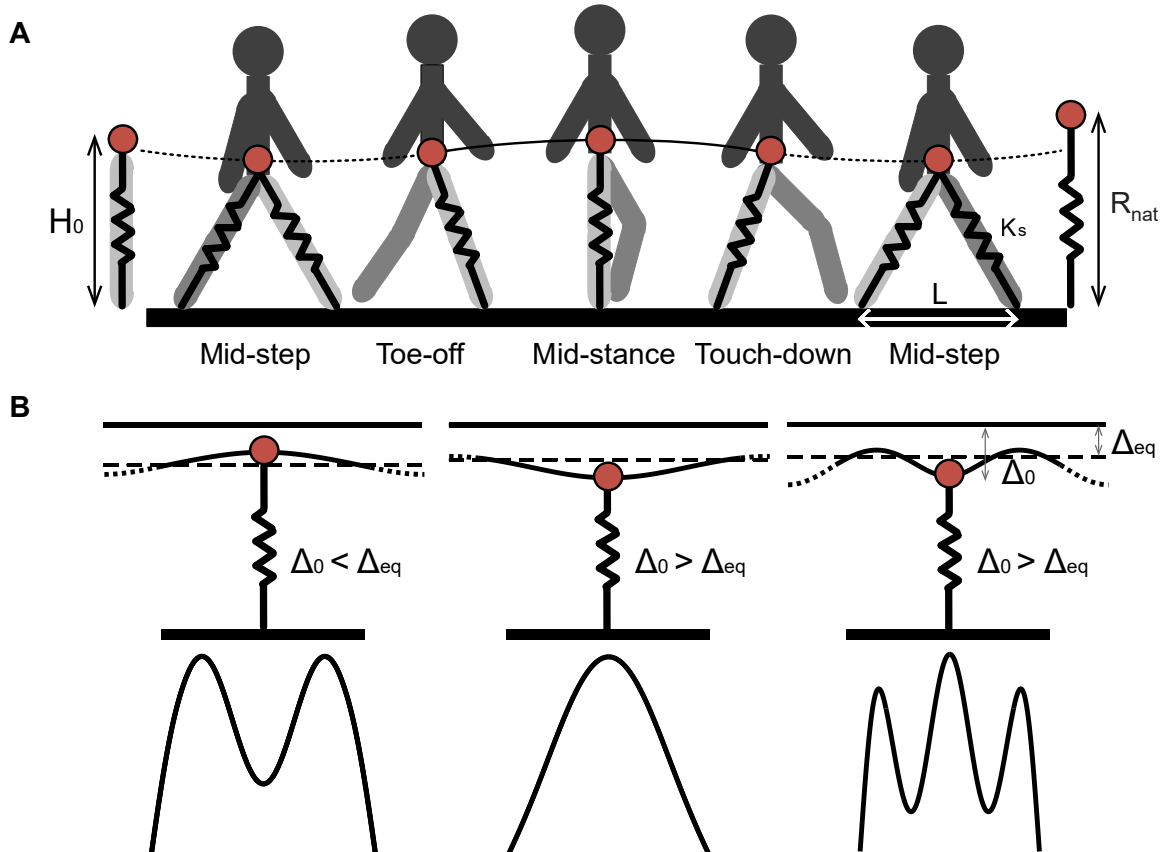


Figure 1. The position of the CoM at mid-stance in relation to the equilibrium point of the spring-mass system determines the GRF profile. A. Gait cycle for normal human walking showing the mid-stance maximum in height and a mid-step minimum in height. The DSLIP model is overlaid on the step cycle. Solid lines and dotted lines represent single and double stance phases respectively. **B.** The top row shows the position of the CoM at mid-stance in relation to the equilibrium position. During human walking (left), the CoM at mid-stance is above this equilibrium point; the resulting vGRF will be at its minimum and produce an M-shaped vGRF. In grounded running (middle), the CoM is at its minimum height below the equilibrium point resulting in the maximum spring contraction/force at mid-stance. Walking with multiple oscillations (right) can have either a maximum or minimum CoM height regarding the number of oscillations. Again with the same logic, the extremums of vGRF profile are defined based on the position of the CoM related to the equilibrium point.

137 2.1 Emergence of different walking gaits and their energetics

138 Different gaits are oscillatory modes of the DSLIP model

139 In previous work, it has already been shown that the DSLIP model can function in multiple

The model's parameters

Parameter	Symbol	Dimensionless form	Relation
Mass	M	N/A	N/A
Acceleration of gravity	g	N/A	N/A
Weight	W	N/A	$W = Mg$
Natural spring length	R_{nat}	N/A	N/A
Time	t	τ	$\tau = t\sqrt{\frac{g}{R_{nat}}}$
Single stance time	t_s	τ_s	$\tau_s = t_s\sqrt{\frac{g}{R_{nat}}}$
Double stance time	t_d	τ_d	$\tau_d = t_d\sqrt{\frac{g}{R_{nat}}}$
Spring stiffness	K_s	γ	$\gamma = \frac{K_s R_{nat}}{W}$
Step length	L	λ	$\lambda = \frac{L}{R_{nat}}$
Radial Coordinate	R	r	$r = \frac{R}{R_{nat}}$
Initial radial coordinate	R_0	r_0	$r_0 = \frac{R_0}{R_{nat}}$
Radial coordinate at equilibrium	R_{eq}	r_{eq}	$r_{eq} = 1 - \frac{1}{\gamma}$
Radial coordinate at transition	R_*	r_*	$r_* = \frac{R_*}{R_{nat}}$
Height of CoM	H	h	$h = \frac{H}{R_{nat}}$
Height of CoM at mid-stance	H_0	h_0	$h_0 = \frac{H_0}{R_{nat}}$
Spring contraction	Δ	δ	$\delta = 1 - r$
Initial spring contraction	Δ_0	δ_0	$\delta_0 = 1 - r_0$
Spring contraction at equilibrium	Δ_{eq}	δ_{eq}	$\delta_{eq} = \frac{1}{\gamma}$
Spring contraction at transition	Δ_*	δ_*	$\delta_* = 1 - r_*$
Angular coordinate	θ	θ	N/A
Angular coordinate at transition	θ_*	θ_*	N/A
Initial angular velocity	$\dot{\theta}_0$	Ω_0	$\Omega_0 = \dot{\theta}_0\sqrt{\frac{g}{R_{nat}}}$
Maximal Spring Energy	E	ϵ	$\epsilon = \frac{E}{MgR_{nat}} = \frac{1}{2}\gamma\delta_{max}^2$
Oscillation frequency	N/A	ω	$\omega = \sqrt{\gamma}$
Oscillation phase	N/A	ϕ	$\phi = \omega t$
Oscillation phase at transition	N/A	ϕ_*	N/A
Horizontal displacement of the CoM	X_{com}	x	$x = \frac{X_{com}}{R_{nat}}$
Vertical displacement of the CoM	Y_{com}	y	$y = \frac{Y_{com}}{R_{nat}}$
Average CoM's speed	V_{com}	v	$v = \frac{V_{com}}{\sqrt{gR_{nat}}}$
Froude number	N/A	Fr	$Fr = \left(\frac{\lambda}{\tau_s + \tau_d}\right)^2$
Horizontal velocity at transition	N/A	v_{x_*}	$v_{x_*} \approx (1 - \delta_*)\Omega_0 \cos \theta_*$
Vertical velocity at transition	N/A	v_{y_*}	$v_{y_*} \approx -(1 - \delta_*)\Omega_0 \sin \theta_*$
Vertical acceleration at transition	N/A	a_{y_*}	$a_{y_*} \approx \gamma\delta_* \cos \theta_* - 1$

140 modes (Geyer et al., 2006; Gan et al., 2018; Andrada et al., 2020; Ding et al., 2022; Mauersberger
141 et al., 2022); these modes include common modes of animal locomotion. These different modes
142 arise from different positions of the CoM in relation to the equilibrium length of the spring (Figure
143 1). To describe the different modes, instead of leg length, it is more convenient to introduce the
144 spring compression, Δ , via $R = R_{nat} - \Delta$. Each mode is an oscillation around the fixed point,

145 $R = R_{eq} = R_{nat} - \Delta_{eq}$, of the spring-mass system given by the Δ where the spring force balances
146 gravity, $\Delta_{eq} = Mg/K_s$, where M is the mass of the subject. Assuming symmetry, at mid-stance the
147 radial coordinate and the height must be either at a maximum or a minimum. At the take-off point,
148 the leg reaches its maximal length or the natural length, R_{nat} . Whether the mid-stance height is at
149 a maximum or minimum is determined by the relationship between the compression at mid-stance,
150 Δ_0 , and Δ_{eq} : If $\Delta_0 > \Delta_{eq}$, the weight is larger than the spring force at mid-stance, the net vertical
151 force points downwards, the second derivative of the height at mid-stance, \ddot{H}_0 , is negative, and the
152 CoM must go down, resulting in a maximum in height and leg length. Thereafter, it must undergo
153 approximately an integral number of oscillations before take-off. Normal human walking with its
154 mid-stance maximum in height is the most common gait of this kind with approximately a single
155 radial oscillation between the mid-stance and take-off (Figure 1B, left).

156 In contrast, if the leg starts below the equilibrium, $\Delta_0 < \Delta_{eq}$, the spring force is larger than the
157 weight, leading to an upward net vertical force, $\ddot{H}_0 > 0$, and therefore a minimum in height and
158 leg length. The radial coordinate undergoes approximately half-integral oscillations before take-off,
159 Figure 1B, middle. The lowest oscillatory mode with approximately half of an oscillation corresponds
160 to the grounded running gait that is employed over a limited speed range in humans but over a large
161 range of speed in some birds ((Andrada et al., 2013b, 2020; Davis et al., 2020). In Figure 1B, right,
162 we also show gait patterns of this type with more than one vertical oscillation.

163 The possible gait patterns and the ranges over which they are found, when we have at most
164 one oscillation, are summarized in Figure 2. We have used dimensionless quantities in Figure 2
165 that will be introduced shortly. As we just explained, the different modes of DSLIP depend on
166 the height of the CoM, H_0 , at midstance in relation to the equilibrium height R_{eq} which in turn
167 depends on the angular speed at mid-stance, and K_s . However, due to the centrifugal force resulting
168 from the angular motion, this transition occurs at a CoM height, H_0 , that is slightly higher than
169 the equilibrium height (see Appendix A for a detailed derivation). Due to the centrifugal force,
170 apart from the normal walking mode, there is a small range of Δ_0 values for which the gait has
171 a mid-stance maximum in height but not an M-shaped GRF. We refer to this gait as Inverted
172 walking. Finally, there is a large range of values where grounded running, with a height minimum
173 and inverted “U”-shaped vGRF maximum, is observed, consistent with theoretical work and the fact
174 that many animals show grounded running (Andrada et al., 2013b; Blickhan et al., 2018; Andrada
175 et al., 2020). The grounded running and inverted walking gaits are together referred to as inverted
176 gaits as they both have an inverted “U”-shaped vGRF maximum, as opposed to the “M” shape
177 observed in normal walking.

178 Gait parameter space

179 To evaluate the exact ranges we found limit cycle solutions. A priori, there are five dimensional
180 parameters that control the evolution of a symmetric gait: stiffness and natural length of the leg
181 spring, K_s and R_{nat} , respectively, the step length, L , and the height and angular velocity at mid-
182 stance, H_0 and $\dot{\theta}_0$, respectively. Together, these five parameters completely specify a symmetric
183 walking trajectory for CoM. We note that time-reversal symmetry requires that at mid-stance and
184 mid-step, \dot{H} must be zero, or the height must be at a maximum or minimum. Typically, as the
185 CoM evolves and reaches mid-step, \dot{H} will not be zero, a condition that is required for a symmetric
186 gait cycle. Imposing $\dot{H} = 0$ at the mid-step, provides an additional constraint, leaving only four
187 independent parameters among $\{K_s, R_{nat}, L, H_0, \dot{\theta}_0\}$ that now uniquely parametrizes limit cycles.
188 To simplify the analysis further, we used dimensionless quantities (by setting $R_{nat} = 1$): the dimen-
189 sionless angular speed and length contraction at the mid-stance, Ω_0 and δ_0 , the dimensionless spring
190 constant, γ , and relative step length, λ . Of these four, only three are independent due to the limit
191 cycle requirement.

192 The range of speeds, expressed as Froude number, Fr , the square of the dimensionless average
193 velocity (approximately equals Ω_0^2), over which limit cycle walking is possible at a given λ is shown
194 in Figure 3A. Limit cycles with M-shaped vGRF are found over the range of speeds over which







Gait	CoM height	GRFs	$\gamma\delta_0$ range
Normal walking	Max 	Min 	$0 < \gamma\delta_0 \leq 1 - \Omega_0^2$
Inverted walking	Max 	Max 	$1 - \Omega_0^2 < \gamma\delta_0 \leq 1$
Grounded running	Min 	Max 	$1 < \gamma\delta_0$

Figure 2. vGRFs and CoM trajectories for different gaits with at most a single contraction-expansion cycle between mid-stance and mid-step and the limits within which each is supposed to occur. The range over which different gaits are observed depends mostly on whether the spring is compressed more or less than the compression necessary to balance the gravitation force. The Ω_0^2 term compensates for the centripetal acceleration and will be small for most walking speeds.

195 humans typically walk. M-shaped vGRF is possible at low speeds with a DSLIP model but not at
 196 the highest speed observed during M-shaped human walking. That DSLIP cannot model M-shaped
 197 walking at the higher end of walking speeds is a well-known limitation of the DSLIP model (Geyer,
 198 2005; Geyer et al., 2006; Lipfert et al., 2012; Mauersberger et al., 2022; Lin et al., 2023) that we
 199 will explore in the next section. Modes with higher oscillations are found only at low speeds (orange
 200 region in Figure 3A). as going through multiple oscillations takes time, increases stance duration,
 201 and decreases speed.

202 The range of speeds for which a single-humped vGRF (inverted gaits) was observed is more ex-
 203 tensive than the M-shaped vGRF. At low speeds, both the M-shaped vGRF and the inverted force
 204 profiles are possible using different γ values. However, only the inverted force profile is possible at
 205 high Froude numbers. Part of this regime (green area) corresponds to grounded running. Consistent
 206 with grounded running observed in humans and other bipeds (Andrada et al., 2013b; Blickhan et al.,
 207 2018; Andrada et al., 2020; Davis et al., 2020), the spring constant decreases as the gait transitions
 208 from normal walking to grounded running.

209 **Normal walking gait with “M”-shaped vGRF are preferred because they are energeti-**
 210 **cally efficient**

Why do humans choose M-shaped GRFs during walking despite other modes being accessible? A possible reason is that the normal gait is energetically most efficient. Although DSLIP itself is a conservative model, the spring compression modeled by DSLIP will require work that will be proportional to the energy stored in the SLIP spring. Thus one can use the maximum spring energy stored as a proxy for energy cost of transport during the given walking step. Now, the maximal stored energy is given by

$$\epsilon = \frac{1}{2}\gamma\delta_{\max}^2. \quad (2.1)$$

The stored energy for a given walking speed, Ω_0 , for the normal and inverted gaits can be estimated. For the normal gait, $\delta_{\max} \approx 2/\gamma - \delta_0$, while in the inverted gaits, $\delta_{\max} \approx \delta_0 > 1/\gamma$ (Figure 1). In

the normal gait, the minimum ϵ is achieved by choosing $\delta_0 \rightarrow 1/\gamma \Rightarrow \delta_{\max} \rightarrow 1/\gamma$, so that

$$\epsilon_{\min, \text{normal}} \approx \frac{1}{2\gamma}. \quad (2.2)$$

Since $\delta_0 > 1/\gamma$ in the inverted gaits ϵ is minimized as $\delta_0 \rightarrow 1/\gamma$ as well. Note that for the normal gait $1/\gamma$ is the largest value of δ_0 , while for the inverted gait, it is the lowest.

$$\epsilon_{\min, \text{inverted}} = \frac{1}{2}\gamma\delta_0^2 = \frac{1}{2\gamma}. \quad (2.3)$$

211 For a given speed, the expression for the minimum stored energy is the same for both gaits, and is
 212 inversely proportional to γ . Therefore, the gait with higher γ is preferred. That the normal gait is a
 213 high stiffness gait is observed in Figure 3A. The same can be inferred intuitively: The take-off angle,
 214 θ_{off} , does not change very much between different walking trajectories. Thus the time, $\theta_{\text{off}}/\Omega_0$,
 215 that a leg is on the ground stays approximately the same as long as the walking speed is the same.
 216 However, in this time, during normal walking the radial coordinate must oscillate once, while in the
 217 grounded running gait it only has to undergo half an oscillation. Since oscillation frequency goes as
 218 the square root of stiffness, γ , this means that the normal walking gait must have a larger stiffness,
 219 and is thus preferred over the inverted gaits.

220 To quantitatively test this idea, we evaluated the ϵ over the entire space where we have limit
 221 cycle solutions and ϵ was smaller for the normal gait compared to the inverted gaits (Figure 3B)
 222 for the same speed. Therefore, M-shaped vGRFs are preferable to grounded running because it
 223 minimizes energy. A similar argument, however, does suggest that multiple oscillatory modes would
 224 have even higher stiffness and, therefore, should be preferred over the normal gait. So why don't
 225 we observe these gaits more frequently? One reason is that each gait (except the grounded running
 226 gait) has a maximum attainable speed, and the higher the number of oscillations, the smaller this
 227 speed-bound. Another possible reason is that the higher oscillatory modes require a much larger
 228 stiffness, making them biologically undesirable. Within the preferred speed range of human walking,
 229 higher oscillatory modes are not available (or have very large stiffness), making the normal walking
 230 gait the most energy-efficient gait.

This analysis above ignores the energy used to propel the swing leg; approximate assessment of
 the energetics of the swing phase show that normal gait will be preferred. It has been previously
 proposed that the swing energy is $\propto \nu^4$, where $\nu = 1/(\tau_s)$ is the angular frequency of the swing leg,
 and τ_s is the dimensionless time for the single stance/swing phase (Kuo et al., 2005). For a given
 angular speed, the energy will diminish steeply with $\theta_* \propto \tau_s$, or

$$\epsilon_{\text{swing}} \propto \frac{1}{\theta_*^4}, \quad (2.4)$$

231 where θ_* is the angular coordinate at the transition from the first single stance to the double stance.
 232 For geometrical reasons, just like θ_{off} , θ_* doesn't vary much between different gaits, but it does
 233 increase slightly (Figure 4B) as one decreases δ_* . Since an increase in γ decreases δ_* , gaits with
 234 higher γ are preferred.

235 To investigate the range of speed allowed using the M-shaped GRF pattern, we found the limit
 236 cycles for the range of relative step lengths (λ) in our experimental data. The allowed region for M-
 237 shaped (normal human walking) (Figure 3C) shows that as λ decreases, the lowest value of γ allowed
 238 increases. The maximum and minimum Froude numbers (Fr) (Figure 3D) show that DSLIP is a
 239 good model at lower speeds but is limited at higher speeds. The range of allowed speeds is low even
 240 after considering different λ values. Compared to the previous study (Antoniak et al., 2019) which
 241 assessed the range of Fr numbers allowed using constraints on the single stance, i.e., without any
 242 requirement for limit cycles (Antoniak et al., 2019), the allowed speed is not altered at the lower
 243 end of the speed range but is altered at the higher end of the speed range. Essentially, DSLIP is an
 244 adequate model for walking at slow speeds whether one considers just the synchronization of radial

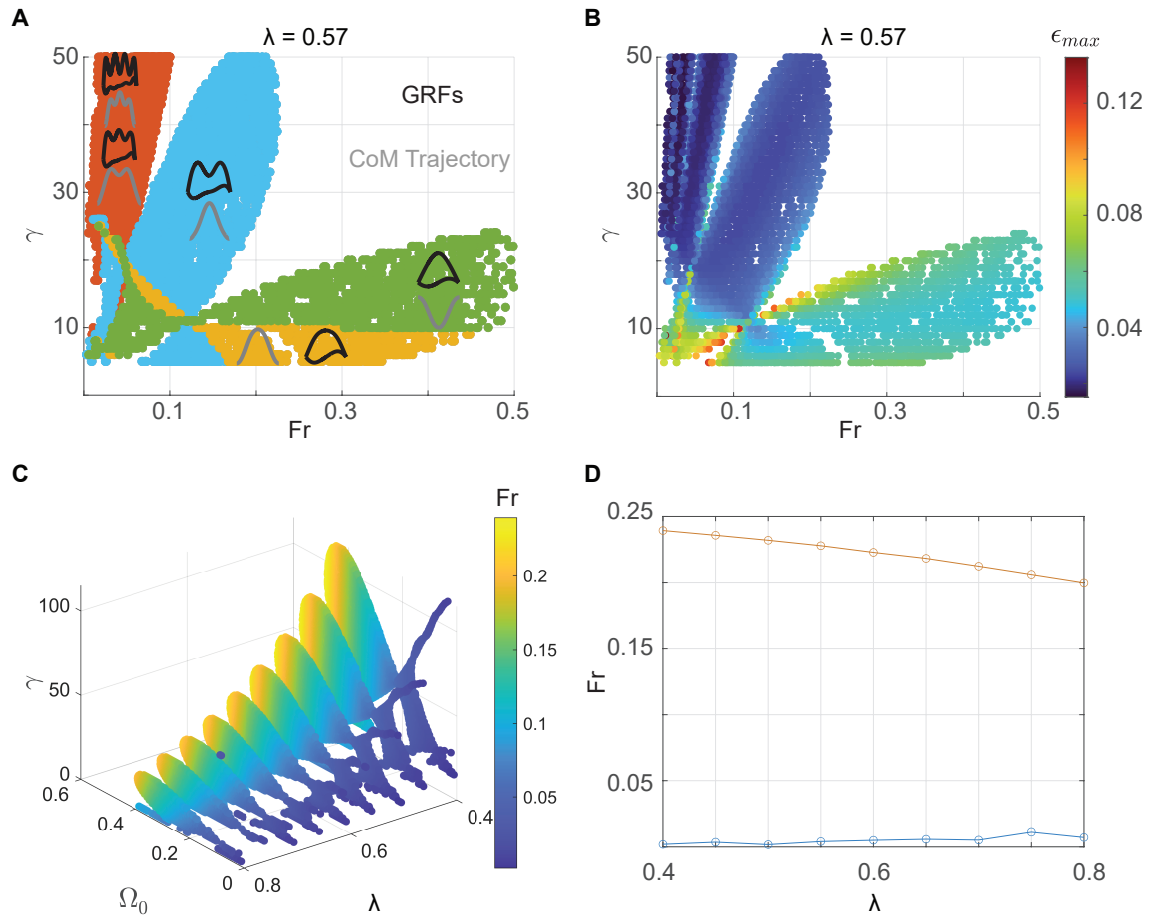


Figure 3. M-shaped walking only occurs over a limited range of speeds over which it is energetically favored. **A.** Solution space for a fixed value of dimensionless step-length, selected according to the best fit to the experimental data for the preferred walking speed of our subject. Four walking modes are shown - three modes from Figure 2 and one mode with multiple oscillations. The vGRF is shown in black, and the CoM profile is in gray. **B.** The same plot as A, with colors specifying the maximum energy stored in the leg during a cycle shows the M-shaped GRF is the most energy efficient over the range of speeds for walking. **C.** The solution space for M-shaped GRFs for different step lengths. The spring stiffness changes with speed. **D.** The M-shaped walking observed in humans is limited to a Fr of 0.25 across step lengths.

245 and horizontal motions during the single stance or the full gait cycle. In contrast, the range of speed
 246 at the high end dramatically decreases when the double stance phase is included, a topic discussed
 247 at length in the next section.

248 **2.2 Constraints from synchronization of radial and angular motion in** 249 **single stance and velocity redirection in double stance limit DSLIP** 250 **normal walking speed**

251 **Synchronization between radial and angular motion during the single stance describes**
 252 **the lower limits of speed possible with M-shaped GRF**

DSLIP correctly predicts that M-shaped GRF walking is only possible for a limited range of speeds. To understand the mechanical constraints that limit the range of speeds for M-shaped walking, we sought an analytical approximation of the DSLIP model. The analytical approximation has two parts that correspond to single and double stance phases, respectively (see Appendix B for details). First, during the single stance phase, we assume that the angular and radial motion are decoupled. When there is no angular motion, and $\theta \approx 0$, the equation of radial motion can be written as

$$\ddot{\delta} = -\gamma \left(\delta - \frac{1}{\gamma} \right) \Rightarrow \delta = \frac{1}{\gamma} + \left(\delta_0 - \frac{1}{\gamma} \right) \cos(\omega t), \text{ where } \omega \equiv \sqrt{\gamma}. \quad (2.5)$$

In other words, δ simply oscillates around its equilibrium value, $1/\gamma$. Further, under the approximation that angular speed is constant, we have

$$\theta = \Omega_0 t. \quad (2.6)$$

The oscillation phase of the radial motion can be defined as

$$\phi \equiv \omega t. \quad (2.7)$$

If ϕ_* and t_* denote the oscillatory phase and time when the single stance transitions to the double stance, at this same time the angular motion must traverse up to the transition angle, θ_* (Figure 4A):

$$t_* = \frac{\phi_*}{\omega} = \frac{\theta_*}{\Omega_0}. \quad (2.8)$$

In other words, γ and Ω_0 are related as

$$\Omega_0 = \left(\frac{\theta_*}{\phi_*} \right) \sqrt{\gamma}. \quad (2.9)$$

This equation implies that as speed (Ω_0) increases, the leg must oscillate faster in the radial direction along the leg-length to keep up, leading to a larger stiffness (γ). The relationship between (Ω_0) and (γ) is more complex as θ_* and ϕ_* are not constants but rather given by (see Appendix B):

$$\sin \theta_* = \frac{\lambda^2 + (1 - \delta_*)^2 - 1}{2(1 - \delta_*)\lambda}, \text{ and } \cos \phi_* = - \left(\frac{\gamma \delta_* - 1}{1 - \gamma \delta_0} \right). \quad (2.10)$$

Briefly, the θ_* equation above results from the transition geometry (Figure 4A), and ϕ_* from Eqn. (2.5). Since δ_* is typically small and ranges between $1/\gamma < \delta_* < 2/\gamma \ll 1$, θ_* does not change much; there is a small increase with decreasing δ_* (Figure 4B). Assuming $\gamma \gg 1$, we have

$$\frac{\lambda}{2} \left(1 - \frac{2}{\gamma \lambda^2} \right) \gtrsim \sin \theta_* \gtrsim \frac{\lambda}{2} \left(1 - \frac{4}{\gamma \lambda^2} \right), \quad (2.11)$$

253 As γ increases, δ_* becomes smaller, and accordingly θ_* increases towards $\sin^{-1}(\lambda/2)$.

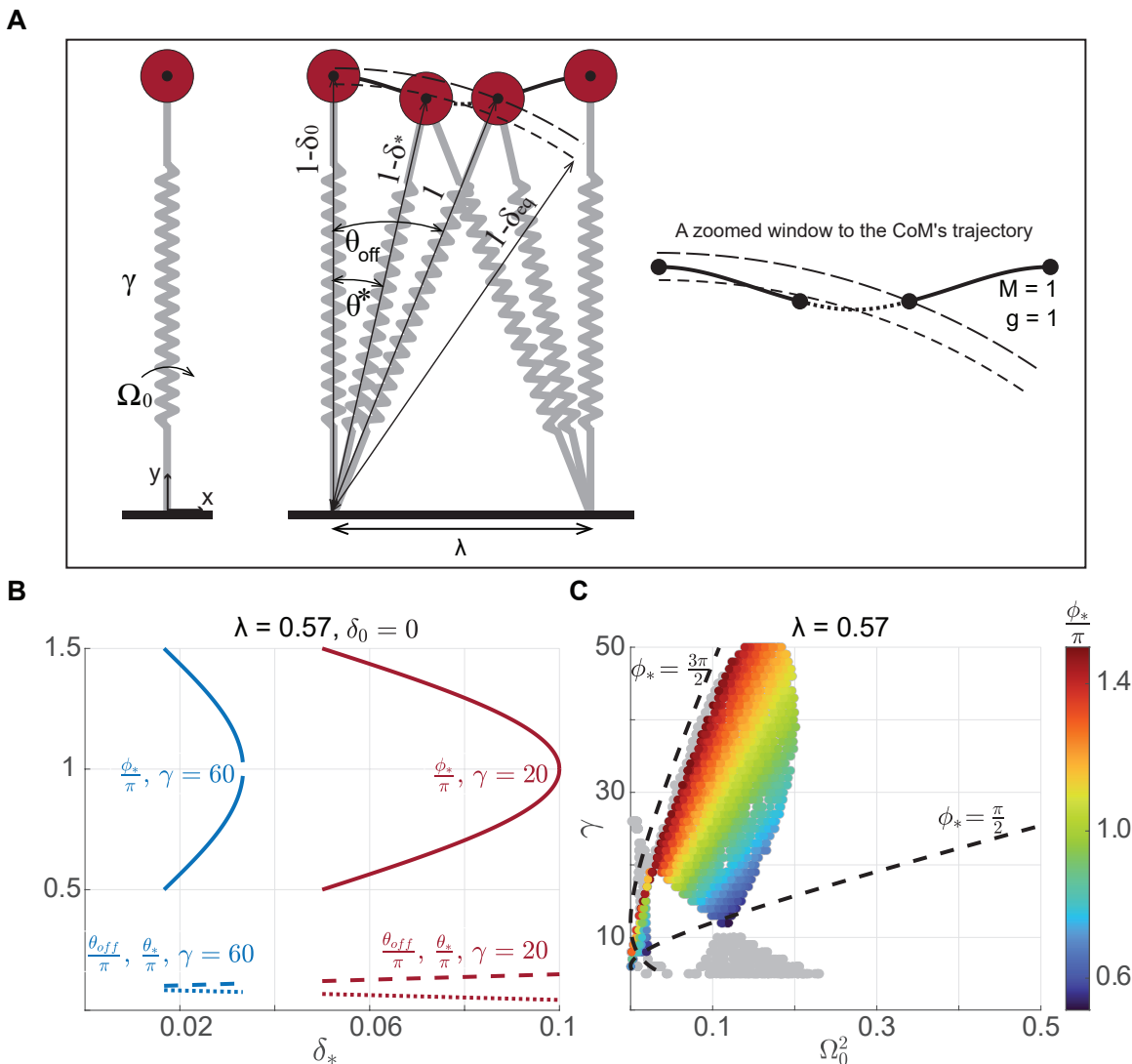


Figure 4. Synchronization between radial and angular motion divides the gaitspace into regions in which different modes are expected. **A.** An example simulation to illustrate synchronization between radial and angular oscillation (middle panel, zoomed version on the right). At a given step-length and leg-contraction at mid-stance, any γ and Ω_0 , only solutions that have synchronized radial and angular motion can become a limit cycle. During the time it takes to travel from midstance to the transition between single and double stance phases - denoted by the starred variables, the angular coordinate must go from midstance to θ_* . The radial coordinate will go from its position between the natural length and equilibrium length at midstance to a position slightly below it. This corresponds to a change in the value of ϕ from 0 at midstance to $\frac{\pi}{2} < \phi_* < \frac{3\pi}{2}$ at the transition. **B.** Two examples based on analytical results show that while ϕ_* approximately accesses the entire range defined for normal walking, θ_{off} and θ_* slightly increases and decreases respectively. **C.** In the figure, only solutions with $\frac{\pi}{2} < \phi_* < \frac{3\pi}{2}$ are shown by color bar; the others are gray. Analytical constraints from synchronization are shown by the dashed line, which is close to the lower bound on speed. However, there is no limit on the upper bound. Note that at high γ , there are no limit cycle solutions close to $\phi_* = \frac{\pi}{2}$.

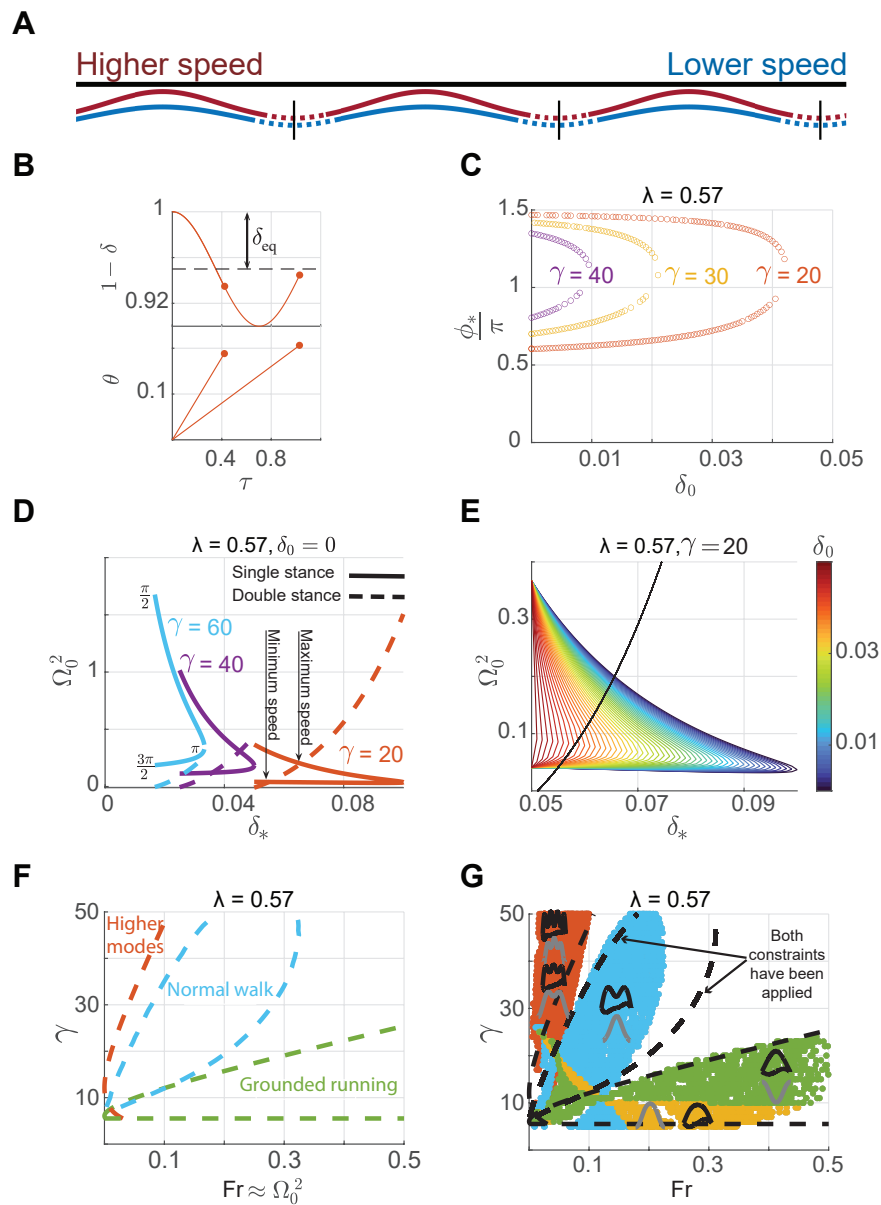


Figure 5. M-shaped walking is limited to low speeds because of a combination of synchronization and velocity redirection constraints. **A.** Two CoM trajectories illustrate the single stance (solid lines) and the double stance (dotted lines) phases. The double stance phase gets shorter with increasing speeds. The vertical black lines specify the mid-step. **B.** The figure shows the approximate evolution of δ and θ during the single stance phase. There are only two solutions once γ , δ_0 , λ are fixed. **C.** The variation of ϕ_* vs. δ_0 for a given step-length for the normal walking gait. By increasing γ , generally the speed increases, and for a given gamma, as the speed increases ϕ_* and δ_0 values get closer to π and zero respectively. **D.** A graphical representation of how single (solid line) and double stance (dashed line) constraints affect the range of possible speeds. Here $\delta_0 = 0$. The highest speed possible (intersection) is much smaller than the highest speed from just single stance considerations (obtained at $\delta_* = \frac{1}{\gamma}$). The difference becomes more with higher stiffness until at the highest stiffness (light blue, $\gamma = 60$), there is no solution (no intersection point). **E.** All solutions for a fixed step-length and stiffness. Note the double stance constraint is independent of δ_0 . **F.** The region of different gait patterns that is estimated by our analytical approximation. The boundaries for normal walking become highly constrained. The other boundaries - for grounded running and higher modes - are a result of single stance constraint alone. **G.** Analytical boundaries of walking solutions from F overlaid on the numerical solution for comparison.

In contrast to the small θ_* range, ϕ_* changes considerably (Figure 4B). When $\cos \phi_*$ is negative (we will justify this in the next subsection), ϕ_* can, a priori, take any value in the range

$$\frac{\pi}{2} < \phi_* < \frac{3\pi}{2} \quad (2.12)$$

254 for a single radial oscillation of the COM. Moreover, (2.10) implies that as δ_* varies, we have two
 255 branches of $\phi_*(\delta_*)$: a branch along which δ_* varies between $1/\gamma$ to $2/\gamma - \delta_0$, and ϕ_* varies between
 256 $\pi/2$ to π , see Figure 4B and another where ϕ_* goes from π to $3\pi/2$ as δ_* varies between $2/\gamma - \delta_0$ to
 257 $1/\gamma$.

We can estimate the speed bounds based on the analytical equations above. It is clear from (2.9) that Ω_0 decreases if ϕ_* increases and θ_* decreases, however, the effect of ϕ_* change is much larger. Thus approximately the lower-bound on speed is attained at $\delta_* \rightarrow 1/\gamma$, and $\phi_* \rightarrow 3\pi/2$ following the upper branch, and yielding

$$\Omega_0 \gtrsim \left(\frac{2}{3\pi} \sin^{-1} \left[\frac{\lambda}{2} \left(1 - \frac{2}{\gamma\lambda^2} \right) \right] \right) \sqrt{\gamma}. \quad (2.13)$$

In a similar way, the upper bound is attained as $\delta_* \rightarrow 1/\gamma$, and $\phi_* \rightarrow \pi/2$:

$$\Omega_0 \lesssim \left(\frac{2}{\pi} \sin^{-1} \left[\frac{\lambda}{2} \left(1 - \frac{2}{\gamma\lambda^2} \right) \right] \right) \sqrt{\gamma}. \quad (2.14)$$

258 The upper and lower bounds resulting from this synchronization are plotted in Figure 4C. The
 259 analytical lower bound derived above matches the simulation results well, implying that the ana-
 260 lytical approximation captures the mechanics well. However, the analytical upper bound does not
 261 match the bounds obtained through simulation. This mismatch occurs because, except for low γ ,
 262 the allowed ϕ_* does not reach $\pi/2$; the allowed ϕ_* deviates further from $\pi/2$ as γ increases. Single
 263 stance mechanics do not constrain the speed for normal walking; instead, as we will see next, con-
 264 straints from double stance limit ϕ_* . This result explains why a previous study that considered only
 265 the single stance phase came to the conclusion that DSLIP can function as a model for walking even
 266 at high speeds (Antoniak et al., 2019).

267 **Limits of DSLIP on speed result from a combination of synchronization and the re-** 268 **quirement to redirect vertical velocity component during the double stance phase**

269 Thus far, we have investigated how synchronization between the horizontal and vertical motions
 270 of the CoM in the single stance phase delineates the regions in the $\gamma - \Omega_0$ space where different gaits
 271 will be observed. The speed range over walking is further constrained by the need to reorient the
 272 velocity vector during double stance: The vertical CoM velocity, which is pointed downwards at the
 273 beginning of the double-support phase, must be redirected upwards by the end of the double-support
 274 phase (Geyer et al., 2006); the required redirection increases with speed. As the speed increases,
 275 this redirection becomes more difficult because the double-support phase becomes shorter, and the
 276 required change in velocity is larger (Figure 5A). We first explain this idea conceptually (Figure 5A):
 277 As speed increases, γ increases as well, and so does the equilibrium height $(1 - 1/\gamma)$. Moreover, as
 278 the radial motion of the CoM is approximately oscillating with an amplitude less than $1/\gamma$, the CoM
 279 trajectory is closer to the natural leg length at higher speeds (Figure 5A), $r \lesssim 1 - 2/\gamma$. Consequently,
 280 the transition geometry dictates that the transition occurs closer to the mid-step at higher speeds,
 281 when the two legs are almost of equal length. This change, in conjunction with increased horizontal
 282 speed, implies that less time is spent in the double support phase. At the same time, as the vertical
 283 component of velocity increases with the overall speed-increase, a larger change in speed is required
 284 at the double-to-single stance transition. A larger speed change in a shorter time necessitates a
 285 larger force to produce a larger acceleration. A back of the envelope calculation is instructive: The
 286 double support phase duration, $t_d \sim \delta\theta/\Omega_0$ keeps shrinking as speed increases while the required
 287 change of vertical velocity necessary during the double support phase increases, $\delta v \sim 2\Omega_0 \sin \theta_*$.

288 Thus the average upward acceleration that one needs, $\sim \delta v/t_d \approx \Omega_0^2 \sin \theta_\star / \delta \theta$, increases with speed.
 289 Crucially, the increased acceleration cannot be produced because the force that can be generated
 290 during normal walking is bounded and is equal to the weight.

291 The above arguments do not incorporate two important effects: First, the oscillatory radial
 292 motion can flatten the trajectory, which, in turn, may reduce the required vertical speed change.
 293 Second, the bound of the maximal radially outward force comes from the approximate oscillatory
 294 dynamics, but obviously, during the double stance phase, both legs are on the ground, which can
 295 therefore provide larger upward forces. Below we provide an approximation and provide an analytic
 296 condition determining the maximum speed bound for the normal walking gait.

297 **Limit Cycle constraint combining the single and double stance synchronization dra-** 298 **matically reduces the solution space**

To estimate the speed bound we will first derive an approximate analytical solution for limit cycle, and then use this analytical solution to estimate the speed bound. The horizontal speed and vertical acceleration are approximately constant during the double-stance phase and equal to their value at the transition between single-stance and double-stance phase: $v_x \approx v_{x\star}$ and $a_y \approx a_{y\star}$. In particular, this implies that at the transition, the vertical acceleration must be upwards to make the velocity redirection possible, or $a_{y\star} > 0$. For an approximately simple harmonic radial oscillation, this occurs during the phase, $\frac{\pi}{2} \lesssim \phi_\star \lesssim \frac{3\pi}{2}$, thereby justifying the assumption (2.12) we made earlier. Using these approximations, and the fact that in the time the leg has to travel horizontally to the mid-step from the transition point, the upward force must be sufficient to bring the downward velocity at transition to zero at mid-step, we can derive the relationship $\Omega_0(\delta_0, \delta_\star, \gamma, \lambda)$ (see Appendix C for the derivation) as

$$\Omega_0^2 = \frac{(\gamma \delta_\star \cos \theta_\star - 1)[\lambda/2 - (1 - \delta_\star) \sin \theta_\star]}{(1 - \delta_\star)^2 \sin \theta_\star \cos \theta_\star} \equiv G_D(\delta_0, \delta_\star, \gamma, \lambda) . \quad (2.15)$$

299 This nonlinear function determining Ω_0 as a function of $\delta_0, \delta_\star, \gamma, \lambda$ describes the speed based on the
 300 double stance constraint. Because $\delta_\star \ll 1$ and θ_\star approximately remain a constant, the first term
 301 (the net upward force) in the numerator is the most important for determining speed, and this will
 302 be important later.

The synchronization relation obtained from the single stance phase is also a function of $\delta_0, \delta_\star, \gamma, \lambda$:

$$\Omega_0^2 = \left(\frac{\theta_\star}{\phi_\star} \right)^2 \gamma \equiv G_S(\delta_0, \delta_\star, \gamma, \lambda) . \quad (2.16)$$

Thus, in order to have a synchronized limit cycle, the four parameters, $\delta_0, \delta_\star, \gamma, \lambda$ must be related,

$$G_D(\delta_0, \delta_\star, \gamma, \lambda) = G_S(\delta_0, \delta_\star, \gamma, \lambda) , \quad (2.17)$$

leaving only three independent parameters, $\delta_0, \gamma, \lambda$. For a given δ_0 and γ , inverting the cosine function in (2.10) while obtaining ϕ_\star results in two branches, referred to here as $\phi_u(\delta_\star) \in (\pi, 3\pi/2)$ and $\phi_l(\delta_\star) \in (\pi/2, \pi)$ (Figure 5C). Accordingly, for a given λ, γ and δ_0 , the upper branch, ϕ_u , leads to a branch with lower speeds from the single stance synchronization condition (2.16),

$$\Omega_0^2 = \left[\frac{\theta_\star(\delta_\star)}{\phi_u(\delta_\star)} \right]^2 \gamma \equiv G_l(\delta_0, \delta_\star, \gamma, \lambda) , \quad (2.18)$$

while the lower branch leads to a branch with higher speeds,

$$\Omega_0^2 = \left[\frac{\theta_\star(\delta_\star)}{\phi_l(\delta_\star)} \right]^2 \gamma \equiv G_u(\delta_0, \delta_\star, \gamma, \lambda) , \quad (2.19)$$

303 So, if the three parameters, $\delta_0, \gamma, \lambda$ are fixed, there are only two possible values of Ω_0 resulting
 304 from two values of ϕ_\star and δ_\star corresponding to two branches of solution (Figure 5B); from a different

perspective, relating single and double-stance dramatically shrinks the solution space from the entire range between $\pi/2$ to $3\pi/2$ for allowed ϕ_* to just two values of ϕ_* (Figure 5C).

Satisfying both single stance and double stance constraints simultaneously is difficult at high speeds and curtails speeds at which walking is possible

Normal walking must satisfy both the single stance and double stance requirement (2.17). The maximum speed occurs at different δ_* and ϕ_* values for the single and double stance: Synchronization during single stance (2.16) suggests that a speed maximum is reached as $\delta_* \rightarrow 1/\gamma$ and $\phi_* \rightarrow \pi/2$ (Figure 5D). However, synchronization during double-stance does not allow $\delta_* \rightarrow 1/\gamma$ and $\phi_* \rightarrow \pi/2$: As $\delta_* \rightarrow 1/\gamma$ - the upward force (the first term within the parenthesis in the numerator of (2.15)) becomes negative and is disallowed (see Figure 4C). Thus, it is not possible for ϕ_* to attain $\pi/2$ (Figure 5C). This inability of ϕ_* to reach $\pi/2$ is also reflected in the simulation results in Figure 4C and becomes worse as γ increases (Figure 4C and 5C). The maximum upward force in the double stance phase occurs at the largest compression possible, $\delta_* \approx 2/\gamma$ when $\phi_* \approx \pi$. In calculating the force δ_* is multiplied by $\gamma \gg 1$, and thus, the effect of δ_* in G_D is dominated by the force term. The maximum speed possible is a compromise between the considerations from single and double stance and the largest speed occurs at a value of δ_* between $\pi/2$ (where the maximum speed from single stance condition occurs) and π (where the maximum speed from double stance condition occurs).

By inspection of (2.10) it is also clear that for a given δ_* , ϕ_* is smallest if $\delta_0 = 0$. Thus, the maximum speed is approximately attained at a δ_* that satisfies both (2.16) and (2.15) for $\delta_0 = 0$. Or,

$$\left(\frac{\theta_*}{\phi_*}\right)^2 \gamma = \frac{(\gamma\delta_* \cos \theta_* - 1)[\lambda/2 - (1 - \delta_*) \sin \theta_*]}{(1 - \delta_*)^2 \sin \theta_* \cos \theta_*}, \quad (2.20)$$

where $\cos \phi_* = -(\gamma\delta_* - 1)$, and θ_* is given by (2.10). (2.20) can be solved to obtain δ_* as a function of λ and γ . Graphically, the solution is given as the intersection between curves depicting equations (2.15) and (2.19) or (2.18) (Figure 5D). The constraining function, G_D , from the double-support does not depend on ϕ_* , and therefore has no branches. It is a monotonically increasing function of δ_* that can intersect both the lower and the higher branches, $G_l(\delta_*)$ and $G_u(\delta_*)$, leading to two possible solutions. The maximum speed is given by the intersection of these two constraints that occur between ϕ_* of $\pi/2$ and π , and is, therefore, lower than the speed possible if we only consider single-stance synchronization. This decrease is exacerbated as γ increases (Figure 5D). For a given λ and large enough γ 's, there are no solutions at all, consistent with our numerical findings (Figure 5D, $\gamma = 60$). The lower bound is also attained when $\delta_0 \rightarrow 0$ as that decreases $\cos \phi_*$ so that ϕ_* can get close to $3\pi/2$ (Figure 5D). The lower bound is reached when δ_* is close to $1/\gamma$, but as argued before, the upper bound δ_* ends up at a compromise value between $1/\gamma$ and $2/\gamma$. The effect of the double-stance constraint on the lower speed bound is much less (Figure 5D).

Essentially the same analysis can be performed for non-zero δ_0 with two limit cycles possible for a given value of δ_0 . More generally, the double-valued nature of $\phi_*(\delta_*)$ leads to a double-valued $\tilde{\delta}_*(\delta_0)$ function (Figure 5E) resulting in a family of curves - one for each δ_0 .

The overall results are summarized in Figures 5F and 5G. The single stance constraint alone divides the gait space into contiguous regions with different oscillatory gaits (Figure 4C). Addition of the double stance constraint limits the region allowed (Figure 5F). The results from the analytical approximation of DSLIP and the actual simulations are overlaid in (Figure 5G). The range of speeds predicted from the analytical consideration (see Appendix C for more details) matches the simulation results closely. The correspondence is particularly close for low speeds. The small discrepancy at the higher speed is likely a result of oversimplification of the dynamics of the double stance phase. However, the critical result is that it is the differing constraints from synchronization in the single and double stance phases that limits the range of speed over which M-shaped walking is possible.

Lowerbound on γ from requirement of a double stance phase

There are two other features of the gaitspace. First, requiring a finite single stance phase places a floor on γ . To change the vertical component of the velocity during the double stance phase at the transition

$$\delta_\star \gtrsim \frac{1}{\gamma} \quad (2.21)$$

We can now use the transition geometry to find a lower bound on γ . As δ_\star increases the transition occurs at smaller θ_\star angles (2.10), also see Figure 4A. Thus if δ_\star is pushed to a very large value by decreasing γ , θ_\star will become zero, and there won't be any single stance phase at all. By setting $\theta_\star = 0$ depicting the extreme configuration when the transition to double stance occurs at the mid-stance, we get

$$\delta_{\star, \max} = 1 - \sqrt{1 - \lambda^2} \gtrsim \frac{1}{\gamma} \Rightarrow \gamma > \gamma_{\min} \equiv \frac{1}{1 - \sqrt{1 - \lambda^2}} \approx \frac{2}{\lambda^2}. \quad (2.22)$$

The analysis above extends to limit cycles with multiple oscillations

The general form of solutions of (B.4) that have a leg-length minimum (or vGRF maximum) at mid-stance can be written as

$$\phi_\star = 2\pi n \pm \arccos\left(\frac{1 - \gamma\delta_\star}{1 - \gamma\delta_0}\right), n \in \{0, 1, \dots\}, \quad (2.23)$$

where we have assumed, $\gamma\delta_\star > 1$, $\gamma\delta_0 > 1$ and $\arccos(\phi)$ is defined as $\cos^{-1}\phi$ with ϕ restricted to the first quadrant, $0 < \phi < \frac{\pi}{2}$. The lowest $n = 0$ mode leads to $0 < \phi_\star < \frac{\pi}{2}$ and corresponds to the inverted gaits¹, the most commonly observed gait among these grounded-running *like* oscillatory modes. In contrast, the normal walking gait, which exhibits a leg-length maximum (or vGRF minimum) at mid-stance is the lowest oscillatory mode ($n=1$) among the normal-walking *like* oscillatory gaits:

$$\phi_\star = \pi(2n - 1) \pm \arccos\left(\frac{\gamma\delta_\star - 1}{1 - \gamma\delta_0}\right), n \in \{1, 2, \dots\}, \quad (2.24)$$

348 where now we have $\gamma\delta_\star > 1$, but $\gamma\delta_0 < 1$. The normal walking gait can thus represent solutions

349 with ϕ_\star either in the second ($\frac{\pi}{2} < \phi_\star < \pi$) or the third ($\pi < \phi_\star < \frac{3\pi}{2}$) quarter of the unit circle.

350 The multiple branches of $\phi_\star(\delta_\star)$ lead to multiple branches of G_S as a function of δ_\star , and eventually
 351 many intersections of G_S with G_D . Thus we can have many limit cycles with the same speed and δ_0
 352 that, nevertheless, belong to different oscillatory gaits. Since the higher oscillatory modes correspond
 353 to lower G_S curves, the allowed speed range keeps decreasing as the number of oscillations increases.

354 There is one gait, the grounded running gait, for which the above approximate strategy fails (and
 355 is also unnecessary), as discussed in Appendix D. Essentially, in the grounded running gait, there
 356 is no longer any need to redirect the velocity in the double stance phase, and hence our analytical
 357 calculations are not valid.

358 2.3 DSLIP is an adequate model for human walking only for a narrow 359 range of speeds

360 The analysis presented in this study thus far show that approximating walking dynamics using a
 361 spring-mass system explains features of walking, such as the use of M-shaped GRFs and the range
 362 of speeds over which humans walk. To further evaluate whether the interactions between the walker
 363 and the substrate can be quantitatively described with a spring-mass model, we next evaluated
 364 how close DSLIP came to describing the kinematics and GRFs during walking. To this end, we fit
 365 DSLIP to human walking data. Using an instrumented treadmill, we collected data for four walking

¹Since ϕ_\star can only be positive, the $\phi_\star \in (-\pi/2, 0)$ is unphysical and absent from the $n = 0$ grounded running gait.

366 speeds - 2.0 mph, 2.5 mph, 3.0 mph, and 3.5 mph (see Supplementary Materials 4.2). Following
367 previous work (Antoniak et al., 2019), we fit both the GRF and CoM kinematics in real-world or
368 dimensional units and individual steps rather than the average data. Briefly, fitting just the GRF
369 in normalized time units provides fallacious results as the R_{nat} determines the natural time scale of
370 a pendulum. Thus varying R_{nat} tunes the natural time scale allowing fits to trajectories for a wide
371 range of speeds. However, this is not biologically feasible as the leg length can only vary within a
372 small range, and within the context of SLIP, R_{nat} is considered to be a fixed parameter. At the
373 same time, choosing the height of the hip marker as the CoM is an overly stringent constraint; the
374 marker for hip height is a good approximation for the movement of the CoM in time but not the
375 exact CoM location. Therefore, we began by determining the optimal R_{nat} for - 2.5 mph - which
376 was the preferred walking speed for the subject (Figure 6A).

377 To this end, we first fit a non-periodic trajectory, i.e., the fits were not constrained to be limit
378 cycles, to each walking step separately, to allow more flexibility and independent assessment of the
379 best fit over 40 steps, thereby increasing statistical power (see Supplementary Materials 4.3.1). In
380 obtaining R_{nat} , we used four values of R_{nat} , these values were selected through trial and error. The
381 vertical GRF was well fit at all selected values of R_{nat} , as was the height of the CoM. The highest
382 value of R_{nat} , 128 cm, was the best fit to the horizontal GRF (Figure 6A and B), and yielded the
383 lowest overall error, and was selected as R_{nat} of 128 cm for limit cycle fits.

384 After fixing R_{nat} , there remained only three free parameters that determine a limit cycle; two
385 of them - the average step length and speed were fixed by constraining them to match the exper-
386 imentally observed step length and step time. The remaining parameter is selected as the average
387 minimum vGRF over the single stance phase, which can be directly calculated from the data as well.
388 This parameter captures an essential feature of the vertical ground reaction forces that characterizes
389 its “M”-shape profile and therefore seemed important to us. For more details related to optimization
390 methods, please refer to Supplementary Materials 4.3.2.

391 One example of the limit cycle fit is shown in Figure 6C. A single limit cycle closely describes
392 the entire sequence of steps rather than the average step as is typically done; as a consequence, the
393 limit cycle fits some steps better than others. As an example, the fourth step, which is slower than
394 the optimized limit cycle, does not fit well; but this delay is corrected by faster steps later in the
395 sequence (Figure 6C). Overall, a single limit cycle optimized to fit the entire sequence of steps fits
396 the data well and implies that DSLIP is an excellent model for walking at the preferred speed.

397 Typical single step fits, one for each of the four speeds, are shown in Figure 7A. Walking at 2.5
398 mph is best modeled by DSLIP; at this speed, the optimized limit cycle tracks important dynamical
399 features such as the step length, speed, vGRF, and the single stance time (Figure S1D). The model
400 still produces reasonable fits at both 2.0 mph and 3.0 mph, but the fits deteriorate at these speeds.
401 At 2.0 mph, the best-fit model has a longer single stance time; the fitted vGRF oscillates somewhat
402 more than the empirical data. The nature of the deviation is different at 3.0 mph where the model
403 has a lower minimum in vGRF compared to the subject, and much larger oscillations of the vertical
404 motion of the CoM. The model completely fails at 3.5 mph as the minima in the vGRF is close to
405 zero. The average of total errors from GRFs and CoM kinematics along with parameters of optimized
406 limit cycles, are shown in Figure 7B. The total error validates our qualitative observations above.
407 The median error for fits at 2.0, 2.5, and 3.0 mph are at or below ten percent but are much larger
408 for fits at 3.5 mph.

409 Surprisingly, the best-fit spring constant is higher for 2.0 mph (Figure 8A); this finding provides
410 one important clue regarding why DSLIP works as a great model for walking at 2.5 mph and not
411 other speeds. The higher spring constant is unexpected because most previous work has shown that
412 the spring constant decreases as the speed decreases (Farley and Gonzalez, 1996; Kim and Park,
413 2011). Indeed, the spring constant for the single stance phase, as directly inferred from force-length
414 curve, decreases with speed (Figure S2). At the step length used by our subject to walk at 2.0
415 mph, there are no limit cycle solutions for this spring constant (Figure 8B) and therefore the spring

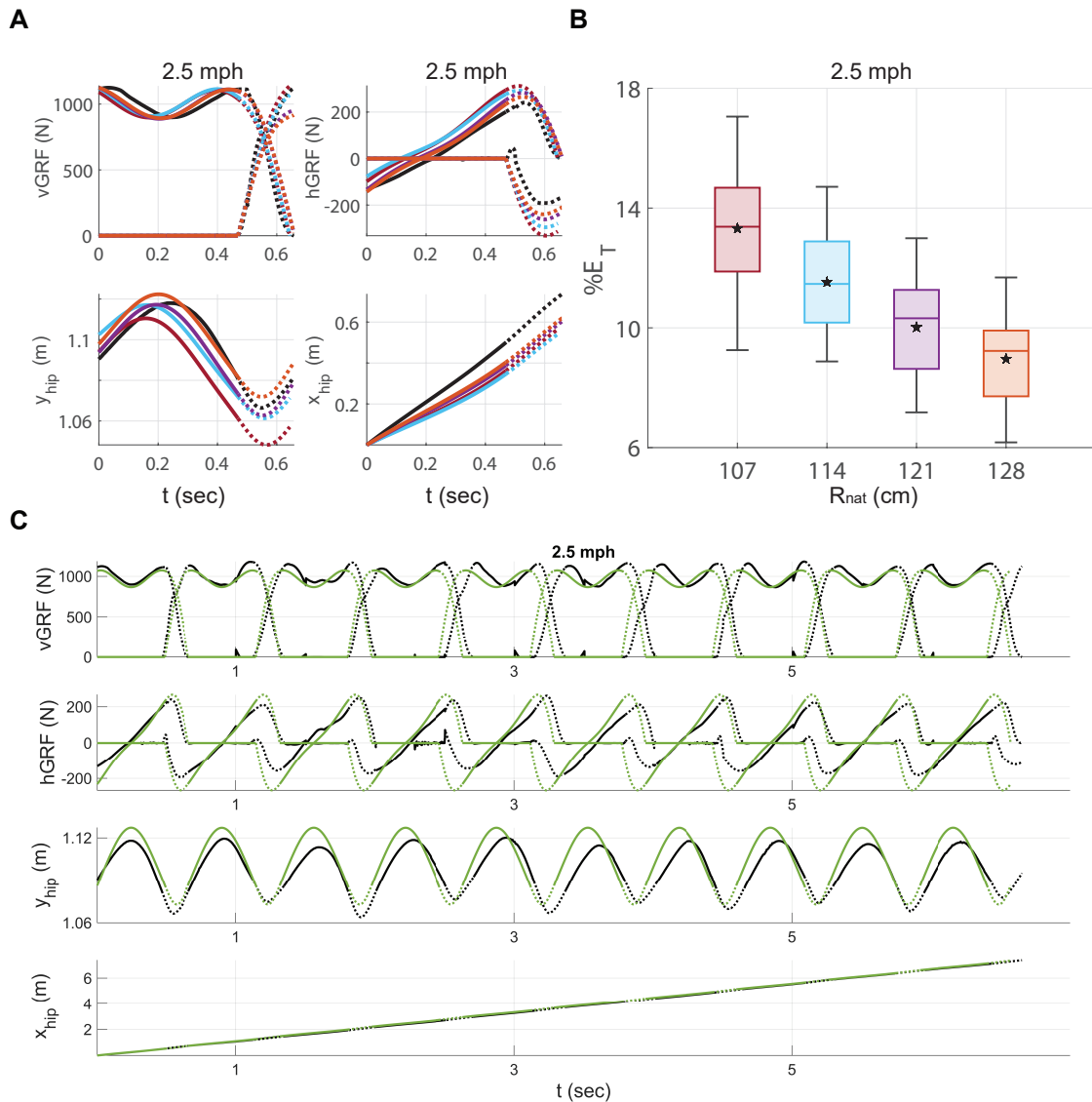


Figure 6. DSLIP is an excellent model for human walking over a narrow range of speeds. **A.** Since the hip marker may not be exactly at the CoM, we fit the experimental data (black lines) to a range of heights both smaller and larger than the hip height (colored lines) (see Supplementary Materials 4.3.1). Solid lines and dotted lines represent single and double stance phases respectively. **B.** The total error for each leg length shows that 128 cm has the lowest error. The error is the sum of errors related to the vGRF, hGRF, height, and horizontal displacement of the CoM. **C.** The optimized limit cycle based on $R_{nat} = 128cm$ (green lines) fits well into 10 walking steps. The total error in time is negligible.

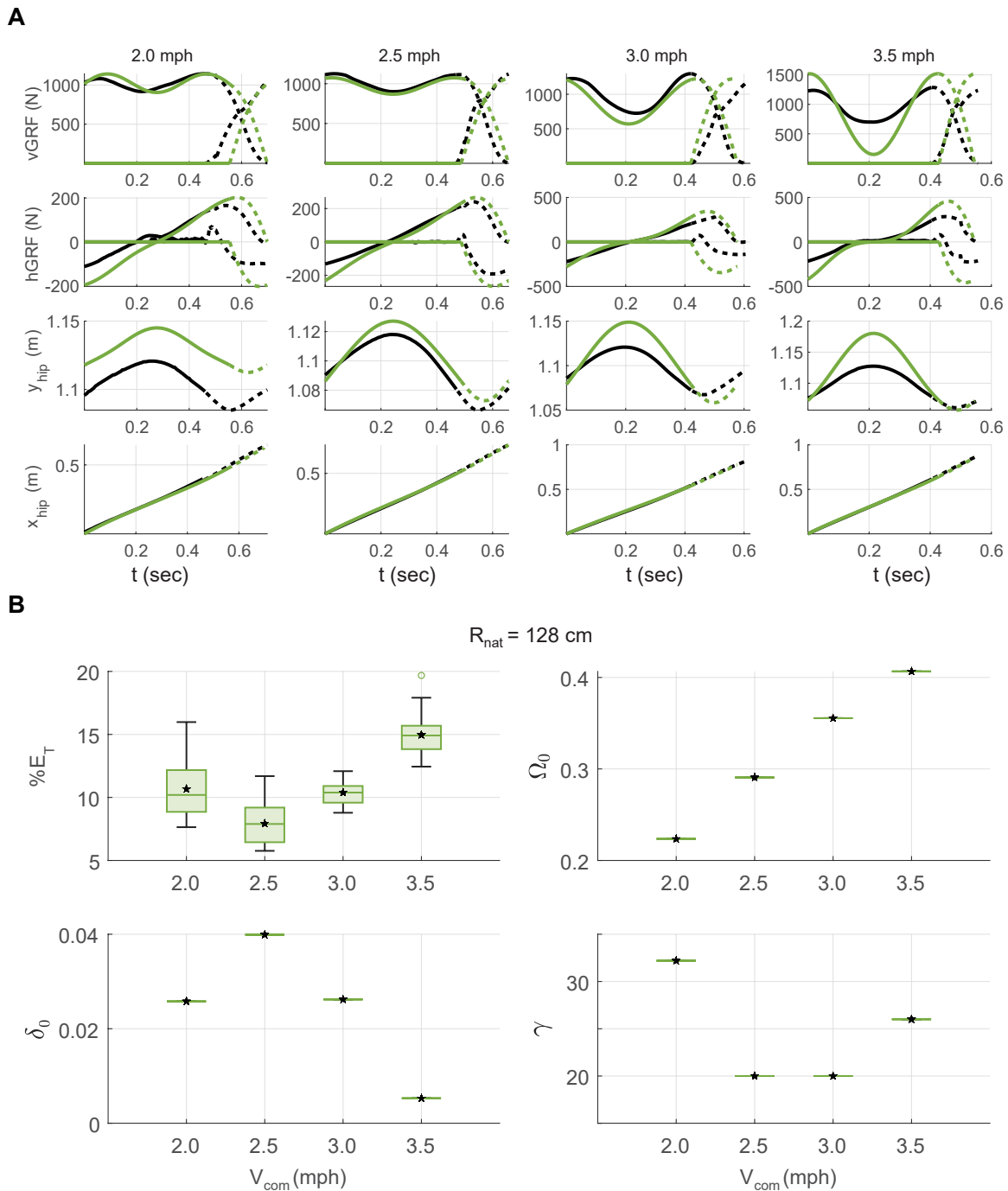


Figure 7. DSLIP fits for both lower and higher than the preferred speed are worse but for distinct reasons. A. Example fits (green lines) and data (black lines). Solid lines and dotted lines represent single and double stance phases respectively. The model and subject have the same step length and speed in all fits. We optimized limit cycles based on the values of vGRF at the mid-stance, which can be considered the only free parameter left. The best fit belongs to the preferred speed (2.5 mph), and the highest speed (3.5 mph) has the worst prediction. **B.** The total errors including GRFs and CoM kinematics along with the parameters of the optimized limit cycles for different walking speeds.

416 constant for the best-fit limit cycle is artificially higher. Previous work (Biswas et al., 2018) suggested
417 that at low speeds it becomes increasingly important to model tangential forces. Their introduction
418 may allow one to walk with lower values of γ in this low velocity regime and provide a more accurate
419 description of the dynamics. The force-length relationship (Figure S2) also shows that at 2.5 mph,
420 the spring constant during single and double stance phases are similar. This similarity can explain
421 why a DSLIP model which uses a single spring constant is a quantitative model for human walking
422 at that speed. At higher speeds, the spring constants that describe single-stance and double-stance
423 phases become very different, and this difference makes it difficult for the DSLIP model to describe
424 the data. The fits at 3.0 mph, has a stiffness that is approximately the average of the values in
425 the single and double stance phase. As a result the model fit has a smaller γ than suggested from
426 the force-length measurements in the single stance phase. With this smaller stiffness generation of
427 the observed fluctuations in vGRF required a much larger change in the CoM height in the fits as
428 compared to what is observed. In sum, DSLIP seem to function as a quantitative model around the
429 preferred walking speed. At lower speeds, the range of spring constant that can lead to limit cycles
430 shrinks. At higher speeds, the spring constants that describe single and double stance phases are
431 different, making it difficult for DSLIP to model.

432 3 Discussion

433 3.1 A compliant leg is necessary for modeling many features of locomotion 434

435 A model with non-compliant legs – IP – continues to persist as a model for walking. The IP model
436 has been successful in explaining the energetics of walking (Donelan et al., 2002; Kuo, 2002; Kuo
437 et al., 2005). The inability of IP model to describe forces is considered a surmountable limitation.
438 Proponents of IP have argued that this limitation of IP arises from the impulsive nature of work
439 in the IP model, and that if this constraint is relaxed, variations of IP model can recover the M-
440 shaped GRF observed during walking. However, we show here that a compliant leg provides two
441 important advantages. First, by providing a means to relate leg stiffness that controls the amplitude
442 and period of the vertical oscillation to the angular speed of stance progression, they provide an
443 analytical framework rooted in mechanics for analyzing which gaits will be observed. Second, leg
444 compliance also provides a mechanism for understanding limitations faced in the redirection of
445 velocity vector. It is clear from the analysis performed in this study that the challenges with
446 redirecting the velocity vector limits the range of speeds over which humans can walk. We also
447 show here that the energetics of a compliant leg is necessary for understanding why a particular
448 gait, defined by GRF and kinematics, is observed in a given step during walking as well. Its relative
449 simplicity and flexibility make it an ideal jumping board for more complex models of locomotion.

450 3.2 M-shaped GRFs are prevalent because they are energetically efficient

451 An unexplained characteristic of human walking is that humans walk with a M-shaped GRF profile.
452 The M-shaped GRF is observed in other walkers including both bipeds and quadrupeds (Andrada
453 et al., 2013a, 2014; Basu et al., 2019). At the speeds at which humans walk, other modes of walking,
454 such as grounded running, are possible. However, the M-shaped profile is energetically favored. We
455 have shown that the normal walking gait has a stiffer leg as compared to grounded running, which is
456 preferred because a stiff leg results in smaller vertical oscillations and therefore ultimately less work².
457 This same logic would posit that even higher modes of oscillation with even stiffer legs would be
458 more energy efficient than the normal gait. While this is true and we do see that at very slow speeds
459 multi-oscillatory gaits may be preferred (Figure S3), these gaits are not available at typical walking

²While work is proportional to the force, it is proportional to the square of the contraction.

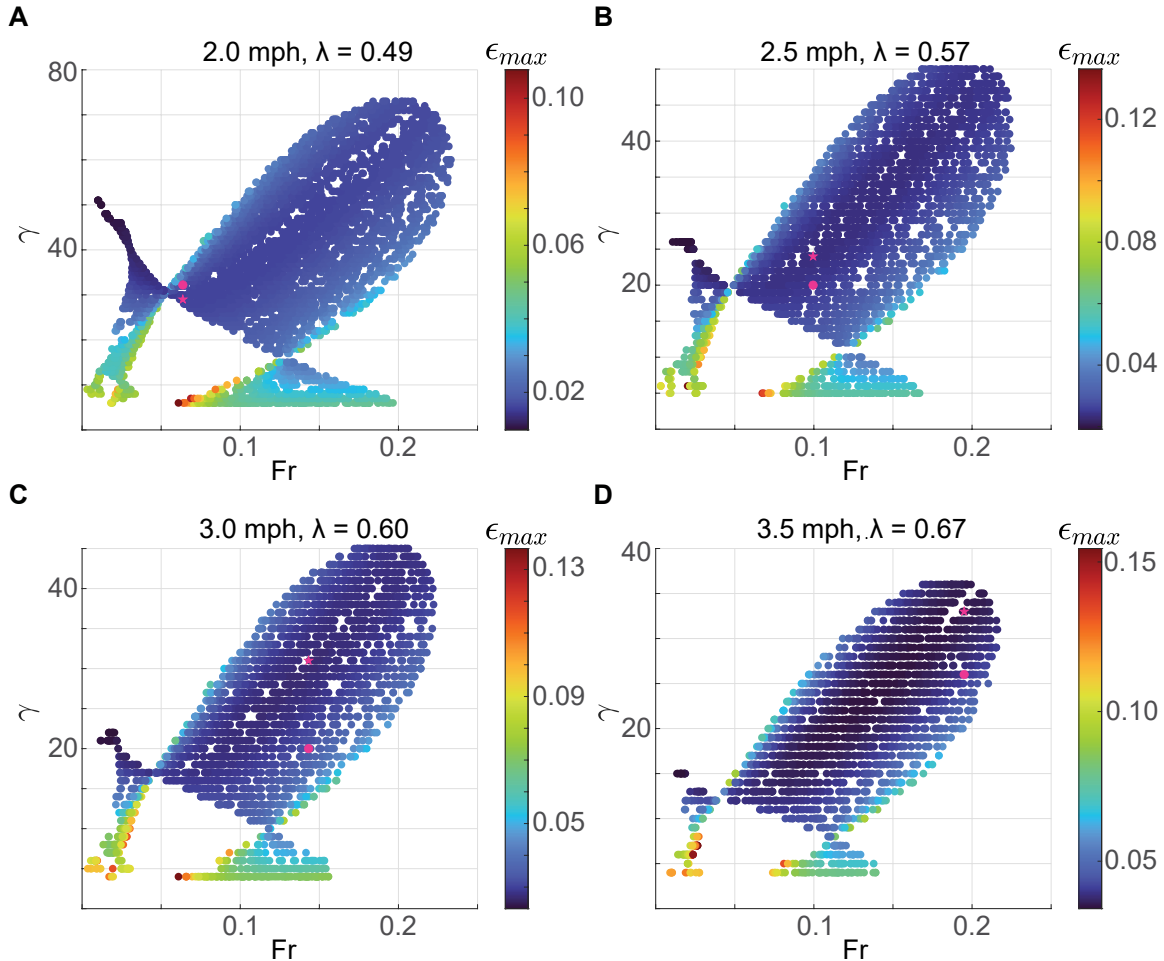


Figure 8. The range of spring constant where a limit cycle is possible likely makes it difficult to obtain good fits for human walking. A, B, C, and D belong to the 2.0, 2.5, 3.0, and 3.5 mph walking speeds of the subject, respectively. The pink circles show the optimized limit cycles based on our method, and the pink stars show the limit cycles with the minimum energy at the same speed. Black crosses demonstrate optimization outputs for non-periodic trajectories. At both 2 mph and 3.5 mph, the optimization solutions are close to the solution boundary.

460 speeds because of a gait-specific speed bound that results from the velocity redirection requirement
461 as we now discuss.

462 **3.3 Gait transition occurs because velocity redirection is difficult**

463 An important issue that has received much attention is gait transitions: at what speeds do they
464 happen and why? One approach to this problem is using the IP model. Walking using an IP
465 model is not possible at high speeds because at high speeds – above Fr of 1 - the centripetal force
466 needed exceeds the gravitational forces. This logic was later modified to take into account the
467 fact that the vertical component of the gravitational force would be lowest near the end of the
468 step. While taking this into account it is possible to produce a walking step with $Fr \sim 0.5$, such
469 steps involves large changes in horizontal speed, completely uncharacteristic of biological walking
470 trajectories (Usherwood, 2005). Analysis in this study using the DSLIP model comes to a very
471 different conclusion. First, even if we take a nuanced approach to walking and impose the condition
472 that walking must have a vGRF minimum at mid-stance, centripetal force does not pose a stringent
473 constraint (see Figure 4C). Moreover, DSLIP makes it possible to walk with gaits that are not possible
474 using the IP model such as the grounded running gait. In sum, adding compliance to the leg removes
475 the appearance of unphysical negative tension force as a reason for gait transition. Our analysis of
476 the DSLIP model suggests a completely different reason for gait transition. Walking with a M-shaped
477 GRF necessitates velocity redirection. Velocity redirection becomes more difficult as speed increases.
478 This inability to perform velocity redirection limits speeds at which walking with M-shaped GRF
479 is possible. There are two options when transitioning from M-shaped walking: Transition can be to
480 other modes without an aerial phase such as grounded running and inverted walking. Alternatively,
481 the transition from M-shaped walking can be to locomotion with an aerial phase. Thus, analysis
482 using DSLIP model suggests two different answers to gait transitions: Transitions out of M-shaped
483 GRFs occur at low speeds, transitions from locomotion without an aerial phase to one with an aerial
484 phase can occur at any speed. As an example, both grounded running and aerial running can occur
485 over a large range of speeds.

486 At what speed aerial running occurs depends on the individual and species. In humans, transi-
487 tions can occur from M-shaped walking to aerial running as is suggested by some. Under certain
488 conditions, there is a small range of speed over which humans walk with a grounded running gait
489 (Shorten and Pisciotta, 2017; Bonnaerens et al., 2019). In many birds, grounded running is preferred
490 over a large range of speeds often exceeding a Fr of 1 (Andrada et al., 2020). Many non-human
491 primates also prefer grounded running (Blickhan et al., 2018). Fast-running insects and spiders
492 prefer grounded running (Reinhardt and Blickhan, 2014). To address which gait is preferred energy
493 estimates for aerial and grounded running at a given speed must be made, which is beyond the scope
494 of this paper.

495 **3.4 Limitations of DSLIP and how they might be overcome**

496 DSLIP is a great conceptual model, but with its simplicity comes some limitations. Although DSLIP
497 does predict that the walk-to-run transition comes from the inability to change the velocity from
498 one step to the next, the speed at which this transition occurs is lower than what is typically
499 observed. DSLIP cannot support walking above a Fr number of 0.25 whereas humans can walk with
500 M-shaped GRF till a Fr number of 0.45 (Kram et al., 1997). There are many mechanisms that might
501 contribute to humans walking at higher Fr numbers. One mechanism is that human legs are not
502 massless, and recoil from the leg swinging forward contributes to velocity redirection (Adamczyk
503 and Kuo, 2009). Another mechanism is that the center of pressure moves forward during stance;
504 this forward movement might increase the range of speeds.

505 All of these processes can be modeled as additions to the SLIP model and aspects of these pro-

506 cesses have been explored by others (Whittington and Thelen, 2009; Lim and Park, 2019; Mauers-
507 berger et al., 2022). Adding features to the model will increase model complexity. If complexity is
508 desired, DSLIP is likely the best base model. However, there are additions that might be highly
509 beneficial without increasing model complexity unduly. One addition is to use a variable spring
510 stiffness. Plotting the relation between change in leg length and force, the slope of which is a sur-
511 rogate for the spring constant, suggests that at high walking speeds both the spring constant and
512 the natural leg length during the single and double stance phases are different (Figure S2). This
513 difference suggests that changing the stiffness and natural length of the spring during the double
514 stance phase may be a mechanism for increasing the speed over which M-shaped GRF walking gaits
515 are possible. Note, that the M-shape is essentially guaranteed by having a minimum at mid-stance
516 during which the dynamics would be identical to DSLIP, and then having a single oscillatory cycle
517 between the mid-stance and take-off.

518 Another mechanism is adding an angular spring. As has been noted previously, net forces during
519 walking do not point along the leg but are more vertical (Maus et al., 2010; Müller et al., 2017;
520 Antoniak et al., 2019). This limitation can be addressed by adding an angular spring as we have
521 proposed earlier (Biswas et al., 2018; Antoniak et al., 2019). An angular spring produces restorative
522 forces such that there is no angular force at mid-stance. The angular forces increase as the leg moves
523 away from mid-stance. As investigated in (Biswas et al., 2018), such angular forces can provide a
524 much wider range of realistic gaits at low speeds.

525 4 Material and Methods

526 In this section, we briefly describe the model, the essential details related to the empirical data, and
527 the numerical techniques to find walking solutions and optimized trajectories.

528 4.1 Walking dynamics of DSLIP

529 In this paper, we reconsider and reevaluate the simplest human walking model introduced by Geyer
530 et al. (Geyer et al., 2006). The model is capable of presenting periodic walking gaits with the fewest
531 set of parameters while keeping important features of human walking such as M-shaped vGRF and
532 CoM trajectory. This model is a basic model for running as well and is able to exhibit other common
533 bipedal gaits with a few modifications (Gan et al., 2018). It is a two degrees of freedom (DoF) model
534 that describes the planar motion of a point mass merely under gravity and spring forces.

535 4.1.1 The equations of motion

The model in its full dimension and dimensionless form is shown in Figure 1A and Figure 4A
respectively. Figure 1A is a schematic but Figure 4A is drawn based on simulation. The model
consists of two mass-less springy legs hinged with a large mass, M , at the hip (CoM). The model
does not include any swing phase dynamics, so the single stance phase is described by just a single
spring with the mass at the top. The natural leg length of the springs is shown by R_{nat} . The leg
stiffness, K_s , and the step length, L , are made dimensionless according to the following equations:

$$\begin{aligned}\gamma &= \frac{K_s R_{nat}}{Mg} \\ \lambda &= \frac{L}{R_{nat}}\end{aligned}\tag{4.25}$$

where g is the gravitational acceleration. To show the dimensionless parameters in the figure, the
values of R_{nat} , M , and g are supposed to be 1. The motion starts from the mid-stance, i.e when

the stance leg stands upright. The dynamics during the single stance phase evolve according to the following equations represented in the Cartesian form:

$$\begin{aligned}\ddot{x} &= \frac{\gamma x(1 - \sqrt{x^2 + y^2})}{\sqrt{x^2 + y^2}} \\ \ddot{y} &= \frac{\gamma y(1 - \sqrt{x^2 + y^2})}{\sqrt{x^2 + y^2}} - 1\end{aligned}\quad (4.26)$$

where x and y show the dimensionless form of horizontal and vertical displacement of the CoM respectively:

$$\begin{aligned}x &= \frac{X_{com}}{R_{nat}} \\ y &= \frac{Y_{com}}{R_{nat}}\end{aligned}\quad (4.27)$$

Also, we made the time dimensionless by using the following relationship:

$$t' = t\sqrt{\frac{g}{R_{nat}}}\quad (4.28)$$

Then, the initial conditions are defined by the position and velocity of the CoM at the mid-stance:

$$\begin{aligned}x_0 &= 0 \\ \dot{x}_0 &= (1 - \delta_0)\Omega_0 \\ y_0 &= 1 - \delta_0 \\ \dot{y}_0 &= -\dot{\delta}_0\end{aligned}\quad (4.29)$$

where δ_0 and Ω_0 are the initial dimensionless spring contraction and angular velocity at the mid-stance, respectively. With appropriate parameters and acceptable initial conditions, the walker is able to continue the single stance phase until the leading leg successfully touches the ground. It is supposed that the touch-down event is recognized by a predefined step length, which can be respected as a very simplified foot placement strategy. At this moment, the following algebraic equation is satisfied by the CoM position:

$$(\lambda - x)^2 + y^2 = 1\quad (4.30)$$

In contrast to rigid inverted pendulum walking models, this impact is conservative, so the CoM begins the double support phase without any energy loss. However, since both the velocity and acceleration of the swing foot get zero, the governing equations of motion switch to the new ones:

$$\begin{aligned}\ddot{x} &= \frac{\gamma x(1 - \sqrt{x^2 + y^2})}{\sqrt{x^2 + y^2}} - \frac{\gamma(\lambda - x)(1 - \sqrt{(\lambda - x)^2 + y^2})}{\sqrt{(\lambda - x)^2 + y^2}} \\ \ddot{y} &= \frac{\gamma y(1 - \sqrt{x^2 + y^2})}{\sqrt{x^2 + y^2}} + \frac{\gamma y(1 - \sqrt{(\lambda - x)^2 + y^2})}{\sqrt{(\lambda - x)^2 + y^2}} - 1\end{aligned}\quad (4.31)$$

When the contact force at the trailing leg gets zero, the leg reaches its natural length and leaves the ground. This moment is called toe-off and is detected by a simple geometric formula:

$$x^2 + y^2 = 1\quad (4.32)$$

Then the single stance phase restarts by resetting the coordinate to the new contact point. In this regard, despite the CoM's velocity continuity, it experiences a discontinuity in its position according to the following equation:

$$x^+ = x^- - \lambda\quad (4.33)$$

where x^+ and x^- are the x-component of CoM just after toe-off and before it respectively. The gait cycle ends when the stance leg re-stands vertically ($x = 0$). Now, we can summarize all equations in a single Poincaré return map which maps the states from i^{th} mid-stance to $(i + 1)^{th}$ mid-stance:

$$q_{i+1} = S(q_i) \quad (4.34)$$

where:

$$q = \{0, \dot{x}_0, y_0, \dot{y}_0\} \quad (4.35)$$

At a fixed point which represents a limit cycle we have:

$$q^* = S(q^*) \quad (4.36)$$

where:

$$q^* = \{0, \dot{x}^*, y^*, \dot{y}^*\} \quad (4.37)$$

536 4.1.2 Parameters and Conditions for symmetric human-like limit cycle walking

Steady-state human walking is so close to a symmetric and periodic locomotion. Employment of this fact helps to reduce the complexity and the number of independent parameters. So it is worthwhile to focus on symmetric limit cycle solutions. To this end, the first derivative of vGRF must be zero at mid-stance. So we have:

$$\dot{F}_y = 0 \implies \dot{y} = 0 \text{ at } x = 0 \quad (4.38)$$

As a result, the general form of initial conditions for equations (4.26) will be:

$$[x_0, \dot{x}_0, y_0, \dot{y}_0] = [0, (1 - \delta_0)\Omega_0, 1 - \delta_0, 0] \quad (4.39)$$

Now, since we just look for limit cycles, there must be a relation between δ_0 and Ω_0 to synchronize the radial displacement of the spring with its rotational movement; so the real number of independent parameters for dimensionless symmetric limit cycle walking will be restricted to three; which can be any three of the following four parameters:

$$P = \{\lambda, \gamma, \Omega_0, \delta_0\} \quad (4.40)$$

Furthermore, to have human-like solutions, i.e. limit cycles with M-shaped vGRF and maximum height profile at the mid-stance, another constraint must be applied to parameters to restrict the solution space. This means that $\ddot{F}_y \geq 0$ and $\ddot{y} \leq 0$ leading to the following inequality:

$$\gamma\delta_0 \leq (1 - \Omega_0^2) \quad (4.41)$$

537 4.1.3 Finding Limit cycles

In general, finding limit cycles is not easy; especially for unstable trajectories. If the DoF is low, and if we have a good estimation of initial conditions, it will be easier to find them. Based on trial and error or using analytical approximations, we can find such an estimation around the desired fixed point which represents a limit cycle. At a fixed point we have:

$$q^* = S(q^*) \quad (4.42)$$

where:

$$q^* = \{0, \dot{x}^*, y^*, 0\} \quad (4.43)$$

This fixed point represents the initial condition that leads to a symmetric periodic gait. To find the fixed point and analyze its stability, we engage a method described in (Wisse et al., 2004). To explain the method in detail, a small perturbation is added to the fixed point at step i as follows:

$$q^* + \Delta q_{i+1} = S(q^* + \Delta q_i) \quad (4.44)$$

Now, by using the Taylor expansion of Poincaré map around the fixed point we have:

$$q^* + \Delta q_{i+1} = S(q^*) + J\Delta q_i \quad (4.45)$$

which results in:

$$\Delta q_{i+1} = J\Delta q_i \quad (4.46)$$

where J is defined as:

$$J = \left. \frac{\partial S}{\partial q} \right|_{q=q^*} \quad (4.47)$$

On the other hand, we have:

$$\Delta q_i = q_i - q^* \quad (4.48)$$

Afterward, based on Eqs. (4.46) and (4.48), we can conclude:

$$q_{i+1} - q_i = (J - I)\Delta q_i \quad (4.49)$$

where I is the identity matrix. Also, employing Eq. (4.34) leads to:

$$S(q_i) - q_i = (J - I)\Delta q_i \quad (4.50)$$

Next, a computer program could be written based on the following algorithm:

$$\begin{aligned} & \textit{Repeat} \\ & \quad \Delta q_i = (J - I)^{-1}(S(q_i) - q_i) \\ & \quad q_i = q_i + \Delta q_i \\ & \textit{Until } |\Delta q_i| < \varepsilon \end{aligned} \quad (4.51)$$

538 where ε is a small disturbance added to the system. Also, the Jacobian matrix, J , can be numer-
 539 ically calculated in every iteration. Now, if the algorithm is convergent, the fixed point and its
 540 corresponding Jacobian matrix simultaneously emerge. Otherwise, either the algorithm must be run
 541 again with a new initial guess or we need to change the system's parameters. Finding the first fixed
 542 point would help to find other fixed points in its vicinity. In this regard, a new initial guess is defined
 543 as a point near the found fixed point. Therefore, trial-and-error is merely necessary to reveal the
 544 first limit cycle.

545 To examine the stability, one also needs to calculate the largest absolute eigenvalue of J , i.e.
 546 $|\Lambda|_{max}$. For this conservative system, the minimum of $|\Lambda|_{max}$ would be 1. That means since
 547 the system is not dissipative, by passing time, a disturbing limit cycle remains perturbed, albeit it
 548 would be very close to the unperturbed trajectory. So stability is guaranteed, although walking is not
 549 asymptotically stable. If $|\Lambda|_{max} > 1$ the limit cycle and its corresponding fixed point are unstable.
 550 Note, in this case, it is feasible to take several successful steps without falling. We implemented the
 551 algorithm in MATLAB and used the 'ode45' function to solve the equations of motion numerically.

552 4.2 Collection of walking data

553 The experimental data is collected from walking of a healthy subject (111 kg weight, 185 cm height)
 554 on a treadmill for one hundred steps at five different speeds, ranging from 1.5 to 3.5 mph, in
 555 increments of 0.5 mph. This range definitely covers the slow, normal, and fast walking of the
 556 subject. It is obtained based on the self-selected, desired speed of the subject, followed by 20% and
 557 40% slower and faster speeds. For data recording, the GRFs were measured by force plates at 1000
 558 Hz, and the hip coordinates were sampled by VICON at 200 Hz. Unfortunately, due to a very high
 559 level of noise or completely useless data, we excluded data related to 1.5 mph from our analysis.
 560 Furthermore, to have a fair comparison among other speeds, we looked for the maximum number of

561 consecutive good strides that are common among all speeds. So, only 40 steps from different time
562 intervals of different speeds were selected.

563 Noise is a part of the data, and especially is observed during measuring the GRFs. To make
564 data smooth without losing any considerable information, we employed 'smoothdata' function in
565 MATLAB, and applied it to the sequence of intervals through all data. These intervals are partitioned
566 with the same size. We used 'sgolay' method (Savitzky-Golay filter). It smooths according to a
567 quadratic polynomial that is fitted over each window of data. This method is more efficient than
568 other existing methods when the data is too rugged and varies quickly.

569 4.3 Fitting DSLIP model to walking data

570 We want to assess DSLIP as a model for human walking by fitting it to the empirical data. In this
571 regard, we employ two different strategies. First, we try to fit the model to each step separately. This
572 gives us an individual non-periodic trajectory for each step that is not connected to the former and
573 latter steps. Second, by averaging empirical data for each walking speed and using the optimized non-
574 periodic trajectories, we try to fit a single limit cycle to all steps. Besides numerous insights about
575 the nature of human walking and the abilities of the model, this procedure proposes a systematic
576 approach to find an appropriate limit cycle in a simple and acceptable way.

577 4.3.1 Optimized non-periodic trajectories

Looking for a non-periodic trajectory means that we have more flexibility. In fact, since we remove
the symmetry and limit cycle constraints, the number of independent parameters for the dimension-
less system increases. Also here, instead of the definition of a step from a mid-stance to a mid-stance,
we can suppose that a step begins with a single stance phase and finishes at the end of the double
support phase. This replacement lets the system parameters vary after the toe-off event instead of
the mid-stance, which is more reasonable. Note we used mid-stance as the Poincaré section just to
simplify finding limit cycles and describing symmetric conditions. According to this new definition,
the system parameters can be reset as follows:

$$P' = \{\lambda, \gamma, \theta_0, \dot{\theta}_0, r_0, \dot{r}_0\} \quad (4.52)$$

578 where, θ_0 , $\dot{\theta}_0$, r_0 , and \dot{r}_0 are dimensionless angular position, angular velocity, radial displacement,
579 and radial velocity of the new stance leg at the beginning of each step, respectively.

580 Furthermore, we are interested in fitting not only GRFs, but also the step length, speed, and
581 position of CoM. To this end, we have to consider the model with full dimension, so R_{nat} must be
582 defined as well. Moreover, because of the unknown location of CoM in the subject, we add a new
583 parameter called D which defines the vertical distance between the hip and CoM. Note $D > 0$ means
584 the CoM is over the hip.

Before doing optimization, we need to define R_{nat} and D ; since these parameters are approxi-
mately constant and do not vary from one step to another. In this regard, we suppose the estimated
 D is within 10 cm from the measured vertical position of the hip at the mid-stance, and the amount
of spring contraction at mid-stance is around 5%; so we have:

$$107 \text{ cm} \leq R_{nat} \leq 128 \text{ cm} \quad (4.53)$$

Based on this inequality, we choose 4 different values for R_{nat} as 107, 114, 121, and 128 cm. Then
the corresponding value of D can be calculated from:

$$R_{nat} = 1.05(D + H_h) \quad (4.54)$$

585 where H_h is the average height of the hip at the mid-stance. To determine other parameters, we
586 need to do optimization. There are several ways to define a cost function. The more complex, the
587 harder to find out the global minimum. So, to avoid local minimums as well as keep the important
588 features of human walking, the optimization algorithm tries to minimize the errors related to the
589 following items:

- 590 • The vGRF at mid-stance
- 591 • The peaks of vGRF
- 592 • The CoM height at mid-stance
- 593 • The single stance time
- 594 • The step time
- 595 • The step length

596 These seven most important characteristics would be easily possible to get minimized by optimizing
597 the system's parameters. Note it is feasible to reduce the dimension of parameter space by fixing λ
598 to the dimensionless step length of the subject, i.e. the step length divided by R_{nat} . Instead, we can
599 calculate the error of the step length by subtracting the model's CoM horizontal displacement from
600 the step length of the subject. This helps to get the optimized trajectory as symmetric as possible.
601 Also since we try to minimize the error related to the step time, it means that we keep the speed of
602 the model the same as the subject.

To do optimization, a computer program was written by using 'Global Optimization Toolbox' of
MATLAB along with 'fmincon' function, 'sqp' algorithm, and 'MultiStart' object. We also determine
the boundaries for our parameters as follows:

$$\begin{aligned} 5 &\leq \gamma \leq 70 \\ 0.05 &\leq \theta_0 \leq 0.50 \\ -0.50 &\leq \dot{\theta}_0 \leq -0.05 \\ -0.15 &\leq r_0 \leq 0 \\ -0.10 &\leq \dot{r}_0 \leq 0.10 \end{aligned} \tag{4.55}$$

603 We did optimization for the specified values of R_{nat} and four different walking speeds, ranging from
604 2.0 mph to 3.5 mph, in increments of 0.5 mph. Then by employing root-mean-square error (RMSE),
605 calculated for vGRF, hGRF, CoM height, and CoM horizontal displacement, we find the best value
606 for R_{nat} . This single value is used to find the optimized limit cycle for each speed separately.

607 4.3.2 Optimized limit cycles

Since limit cycles describe a harmonic motion in a dynamical system, it is not meaningful to look for
them for each step separately. In contrast, by considering human walking as a dynamical system,
it is more acceptable to fit a single limit cycle to all steps. To this end, first, we are interested in
using the information gained from the previously optimized trajectories as a basis. In this regard,
the most important parameters that can be beneficial are R_{nat} and D . Thus, for the optimized limit
cycles, R_{nat} and D are predefined and fixed. Also, λ is chosen based on the average step length of
the subject for each speed divided by R_{nat} . The next parameter is selected as the subject average
speed in its modified form called Froude number, Fr , which is calculated according to the following
equation:

$$Fr = \frac{V_{trd}^2}{R_{nat}g} \tag{4.56}$$

608 where, V_{trd} is the treadmill speed. There is merely one left parameter that must be determined to
609 have a full dimension limit cycle, emulating the GRFs and CoM's trajectory of the subject. Here,
610 we choose the dimensionless form of vGRF at the mid-stance (the minimum vGRF of the subject
611 during the single stance phase divided by the weight of the subject), $\gamma\delta_0$, since it is available from
612 the data. The other choice could be the single stance time; however because we have already kept
613 the step length and the speed of the subject, the period of the cycle is fixed. So instead of tracking
614 another kinematic variable, it would be better to try to fit something from the force diagram. Now,
615 by plotting the solution space for the fixed λ and in $Fr-\gamma\delta_0$ plane, we can choose the limit cycle
616 which has the same λ and Fr as the subject and has the closest location to the empirical data
617 according to the minimum vGRF during the single stance phase. Beyond its simplicity, this is an
618 effective method to judge the model and its ability to predict empirical data.

619 **Acknowledgements:** T.B. was funded by the Howard Hughes Medical Institute. This research was
620 supported by RO1DC015827 (VB), RO1NS097881 (VB) and an NSF CAREER award (IOS-1652647
621 to VB).

622 References

- 623 Adamczyk, P. G. and Kuo, A. D. (2009). Redirection of center-of-mass velocity during the step-to-
624 step transition of human walking. *Journal of Experimental Biology*, 212(16):2668–2678.
- 625 Ahn, A. N., Furrow, E., and Biewener, A. A. (2004). Walking and running in the red-legged running
626 frog, *kassina maculata*. *Journal of Experimental Biology*, 207(3):399–410.
- 627 Andrada, E., Blickhan, R., Ogihara, N., and Rode, C. (2020). Low leg compliance permits grounded
628 running at speeds where the inverted pendulum model gets airborne. *Journal of Theoretical
629 Biology*, 494:110227.
- 630 Andrada, E., Nyakatura, J. A., Bergmann, F., and Blickhan, R. (2013a). Adjustments of global and
631 local hindlimb properties during terrestrial locomotion of the common quail (*coturnix coturnix*).
632 *Journal of Experimental Biology*, 216(20):3906–3916.
- 633 Andrada, E., Rode, C., and Blickhan, R. (2013b). Grounded running in quails: simulations indicate
634 benefits of observed fixed aperture angle between legs before touch-down. *Journal of theoretical
635 biology*, 335:97–107.
- 636 Andrada, E., Rode, C., Sutedja, Y., Nyakatura, J. A., and Blickhan, R. (2014). Trunk orientation
637 causes asymmetries in leg function in small bird terrestrial locomotion. *Proceedings of the Royal
638 Society B: Biological Sciences*, 281(1797):20141405.
- 639 Antoniak, G., Biswas, T., Cortes, N., Sikdar, S., Chun, C., and Bhandawat, V. (2019). Spring-loaded
640 inverted pendulum goes through two contraction-extension cycles during the single-support phase
641 of walking. *Biology open*, 8(6):bio043695.
- 642 Basu, C., Wilson, A. M., and Hutchinson, J. R. (2019). The locomotor kinematics and ground
643 reaction forces of walking giraffes. *Journal of Experimental Biology*, 222(2):jeb159277.
- 644 Biswas, T., Rao, S., and Bhandawat, V. (2018). A simple extension of inverted pendulum template
645 to explain features of slow walking. *Journal of theoretical biology*, 457:112–123.
- 646 Blickhan, R. (1989). The spring-mass model for running and hopping. *Journal of biomechanics*,
647 22(11-12):1217–1227.
- 648 Blickhan, R., Andrada, E., Hirasaki, E., and Ogihara, N. (2018). Global dynamics of
649 bipedal macaques during grounded and aerial running. *Journal of Experimental Biology*,
650 221(24):jeb178897.

- 651 Blickhan, R. and Full, R. (1993). Similarity in multilegged locomotion: bouncing like a monopode.
652 *Journal of Comparative Physiology A*, 173:509–517.
- 653 Bonnaerens, S., Fiers, P., Galle, S., Aerts, P., Frederick, E. C., Kaneko, Y., Derave, W., et al. (2019).
654 Grounded running reduces musculoskeletal loading. *Medicine and Science in Sports and Exercise*,
655 51(4):708–715.
- 656 Buczek, F. L., Cooney, K. M., Walker, M. R., Rainbow, M. J., Concha, M. C., and Sanders, J. O.
657 (2006). Performance of an inverted pendulum model directly applied to normal human gait.
658 *Clinical Biomechanics*, 21(3):288–296.
- 659 Daley, M. A., Felix, G., and Biewener, A. A. (2007). Running stability is enhanced by a proximo-
660 distal gradient in joint neuromechanical control. *Journal of Experimental Biology*, 210(3):383–394.
- 661 Davis, S., Fox, A., Bonacci, J., and Davis, F. (2020). Mechanics, energetics and implementa-
662 tion of grounded running technique: a narrative review. *BMJ Open Sport & Exercise Medicine*,
663 6(1):e000963.
- 664 Ding, J., Moore, T. Y., and Gan, Z. (2022). A template model explains jerboa gait transitions across
665 a broad range of speeds. *Frontiers in Bioengineering and Biotechnology*, 10.
- 666 Donelan, J. M., Kram, R., and Kuo, A. D. (2002). Mechanical work for step-to-step transitions is
667 a major determinant of the metabolic cost of human walking. *Journal of experimental biology*,
668 205(23):3717–3727.
- 669 Farley, C. T. and Gonzalez, O. (1996). Leg stiffness and stride frequency in human running. *Journal*
670 *of biomechanics*, 29(2):181–186.
- 671 Gan, Z., Yesilevskiy, Y., Zaytsev, P., and Remy, C. D. (2018). All common bipedal gaits emerge
672 from a single passive model. *Journal of The Royal Society Interface*, 15(146):20180455.
- 673 Geyer, H. (2005). *Simple models of legged locomotion based on compliant limb behavior*. PhD thesis.
- 674 Geyer, H., Seyfarth, A., and Blickhan, R. (2006). Compliant leg behaviour explains basic dynamics
675 of walking and running. *Proceedings of the Royal Society B: Biological Sciences*, 273(1603):2861–
676 2867.
- 677 Griffin, T. M., Main, R. P., and Farley, C. T. (2004). Biomechanics of quadrupedal walking: how do
678 four-legged animals achieve inverted pendulum-like movements? *Journal of Experimental Biology*,
679 207(20):3545–3558.
- 680 Hubel, T. Y. and Usherwood, J. R. (2015). Children and adults minimise activated muscle volume
681 by selecting gait parameters that balance gross mechanical power and work demands. *Journal of*
682 *Experimental Biology*, 218(18):2830–2839.
- 683 Kim, S. and Park, S. (2011). Leg stiffness increases with speed to modulate gait frequency and
684 propulsion energy. *Journal of biomechanics*, 44(7):1253–1258.
- 685 Kram, R., Domingo, A., and Ferris, D. P. (1997). Effect of reduced gravity on the preferred walk-run
686 transition speed. *The Journal of experimental biology*, 200(4):821–826.
- 687 Kuo, A. D. (2001). A simple model of bipedal walking predicts the preferred speed–step length
688 relationship. *J. Biomech. Eng.*, 123(3):264–269.
- 689 Kuo, A. D. (2002). Energetics of actively powered locomotion using the simplest walking model. *J.*
690 *Biomech. Eng.*, 124(1):113–120.
- 691 Kuo, A. D., Donelan, J. M., and Ruina, A. (2005). Energetic consequences of walking like an inverted
692 pendulum: step-to-step transitions. *Exercise and sport sciences reviews*, 33(2):88–97.

- 693 Lee, C. R. and Farley, C. T. (1998). Determinants of the center of mass trajectory in human walking
694 and running. *Journal of experimental biology*, 201(21):2935–2944.
- 695 Lim, H. and Park, S. (2019). A bipedal compliant walking model generates periodic gait cycles with
696 realistic swing dynamics. *Journal of Biomechanics*, 91:79–84.
- 697 Lin, B., Živanović, S., Zhang, S., Zhang, Q., and Fan, F. (2023). Evaluation of compliant walking
698 locomotion models for civil engineering applications. *Journal of Sound and Vibration*, 561:117815.
- 699 Lipfert, S. W., Günther, M., Renjewski, D., Grimmer, S., and Seyfarth, A. (2012). A model-
700 experiment comparison of system dynamics for human walking and running. *Journal of theoretical*
701 *biology*, 292:11–17.
- 702 Mauersberger, M., Hähnel, F., Wolf, K., Markmiller, J. F., Knorr, A., Krumm, D., and Odenwald,
703 S. (2022). Predicting ground reaction forces of human gait using a simple bipedal spring-mass
704 model. *Royal Society Open Science*, 9(7):211582.
- 705 Maus, H.-M., Lipfert, S., Gross, M., Rummel, J., and Seyfarth, A. (2010). Upright human gait did
706 not provide a major mechanical challenge for our ancestors. *Nature communications*, 1(1):70.
- 707 Maus, H.-M., Revzen, S., Guckenheimer, J., Ludwig, C., Reger, J., and Seyfarth, A. (2015).
708 Constructing predictive models of human running. *Journal of The Royal Society Interface*,
709 12(103):20140899.
- 710 McMahon, T. A. and Cheng, G. C. (1990). The mechanics of running: how does stiffness couple
711 with speed? *Journal of biomechanics*, 23:65–78.
- 712 Müller, R., Rode, C., Aminiaghdam, S., Vielemeyer, J., and Blickhan, R. (2017). Force direction
713 patterns promote whole body stability even in hip-flexed walking, but not upper body stabil-
714 ity in human upright walking. *Proceedings of the Royal Society A: Mathematical, Physical and*
715 *Engineering Sciences*, 473(2207):20170404.
- 716 Nishikawa, K., Biewener, A. A., Aerts, P., Ahn, A. N., Chiel, H. J., Daley, M. A., Daniel, T. L.,
717 Full, R. J., Hale, M. E., Hedrick, T. L., et al. (2007). Neuromechanics: an integrative approach
718 for understanding motor control. *Integrative and comparative biology*, 47(1):16–54.
- 719 Reinhardt, L. and Blickhan, R. (2014). Level locomotion in wood ants: evidence for grounded
720 running. *Journal of Experimental Biology*, 217(13):2358–2370.
- 721 Rummel, J., Blum, Y., and Seyfarth, A. (2010). Robust and efficient walking with spring-like legs.
722 *Bioinspiration & biomimetics*, 5(4):046004.
- 723 Schmitt, D. (1999). Compliant walking in primates. *Journal of Zoology*, 248(2):149–160.
- 724 Shorten, M. and Pisciotta, E. (2017). Running biomechanics: what did we miss? *ISBS Proceedings*
725 *Archive*, 35(1):293.
- 726 Srinivasan, M. (2011). Fifteen observations on the structure of energy-minimizing gaits in many
727 simple biped models. *Journal of The Royal Society Interface*, 8(54):74–98.
- 728 Srinivasan, M. and Ruina, A. (2006). Computer optimization of a minimal biped model discovers
729 walking and running. *Nature*, 439(7072):72–75.
- 730 Usherwood, J. R. (2005). Why not walk faster? *Biology letters*, 1(3):338–341.
- 731 Whittington, B. R. and Thelen, D. G. (2009). A simple mass-spring model with roller feet can
732 induce the ground reactions observed in human walking. *Journal of Biomechanical Engineering*,
733 131(1).
- 734 Wisse, M., Schwab, A. L., and van der Helm, F. C. (2004). Passive dynamic walking model with
735 upper body. *Robotica*, 22(6):681–688.

Supplementary Materials

736

A Single stance dynamics and different gait patterns

737

Let us characterize the different gaits DSLIP can realize that, at most, exhibit a single radial (leg length) oscillation. We can write the equations of motion for the single stance phase in dimensionless polar coordinates (Table 1) centered around the point of ground contact as

$$\ddot{\delta} = -(1 - \delta)\dot{\theta}^2 - \gamma\delta + \cos\theta \quad (\text{A.1})$$

$$\ddot{\theta} = (\sin\theta + 2\delta\dot{\theta})/(1 - \delta) . \quad (\text{A.2})$$

738 where δ represents the dimensionless spring contraction, and θ defines the angular coordinate.

739 For the most part we are going to consider symmetric limit cycles. This means that at the mid-
 740 stance the CoM either has a minimum or a maximum in kinematic variables such as vertical height,
 741 and vGRF. We will show that three different gaits are possible depending upon the height and vGRF
 742 profiles with at most a single radial (leg length) oscillation. The normal gait has a height maximum
 743 and vGRF minimum at mid-stance, while both the inverted gaits (grounded running and inverted
 744 walking) have a vGRF maximum at mid-stance. While the grounded running has a height minimum
 745 at mid-stance, inverted walking has a height maximum similar to normal walking gait. Finally, let
 746 us reiterate (Biswas et al., 2018) that within the DSLIP model there is no provision to have a mid-
 747 stance maximum in horizontal velocity, it always has a minimum. The different gait characteristics
 748 are summarized in the table below along with the relationships between gait parameters that must
 749 be satisfied. We now derive these relationships.

To ascertain the region in parameter space where the different gaits emerge, first consider the vertical acceleration at the mid-stance:

$$\ddot{h}_0 = \gamma\delta_0 - 1 . \quad (\text{A.3})$$

Clearly then to have a maximum in height we must have $\delta_0 < 1/\gamma$. Now the vertical spring force is given by

$$\bar{F}_y = \gamma\delta \cos\theta . \quad (\text{A.4})$$

Using (A.2) we find that at the mid-stance

$$\ddot{\bar{F}}_y = \gamma[1 - \gamma\delta_0 - \Omega_0^2] . \quad (\text{A.5})$$

For \bar{F}_y to have a minimum at the mid-stance then, this must be positive, or

$$\delta_0 \leq \frac{1 - \Omega_0^2}{\gamma} . \quad (\text{A.6})$$

We also note that for a given λ there is an upperbound for δ_0 to have any single stance phase at all, see Fig.?:

$$\delta_0 < 1 - \sqrt{1 - \lambda^2} \equiv \delta_{\max} . \quad (\text{A.7})$$

750 Thus based on the range of δ_0 one can have different gait profiles that we tabulate below:

751

gait	mid-stance height	mid-step height	mid-stance vGRF	mid-step vGRF	mid-stance velocity	δ_0 range
normal walk	maximum	minimum	minimum	maximum	minimum	$0 < \delta_0 < \frac{1 - \Omega_0^2}{\gamma}$
inverted walk	maximum	minimum	maximum	minimum	minimum	$\frac{1 - \Omega_0^2}{\gamma} < \delta_0 < \frac{1}{\gamma}$
grounded run	minimum	maximum	maximum	minimum	minimum	$\frac{1}{\gamma} < \delta_0$

752

753 B Approximate Trajectories

754 Our goal in this subsection is to derive approximate trajectories of the CoM in order to gain analytical
 755 insights into how different parameters must adjust to have a synchronized motion. Also, this will
 756 help us address how well DSLIP is able to capture some of the well-known features of the walking
 757 gait.

758 B.1 Single stance phase

Starting from the dynamical equations in polar coordinates (A.1, A.2), solutions for $\delta(t)$ and $\phi(t)$ were derived in the main manuscript,

$$\begin{aligned}\delta &= \frac{1}{\gamma} + \left(\delta_0 - \frac{1}{\gamma} \right) \cos(\omega t) \\ \theta &= \Omega_0 t\end{aligned}\tag{B.1}$$

759 where we assumed that the angular and radial motion during the single stance phase are effectively
 760 decoupled. The main idea behind this approximation is that for walking trajectories the radial
 761 motion undergoes oscillations around its equilibrium position $\delta_{eq} = 1/\gamma$, and since $\gamma \sim \mathcal{O}(10) -$
 762 $\mathcal{O}(100)$, the oscillations are small. We also assume that the angular/horizontal velocity of CoM
 763 remains approximately constant. Technically, this means that we are ignoring $\dot{\theta}^2$ term as compared
 764 to $(\gamma\dot{\theta})$ in (A.1). Since $\dot{\theta}^2 \sim \Omega_0^2$ and $(\gamma\dot{\theta}) \sim 1$ on an average, this boils down to assuming $\dot{\theta}^2 \ll 1$
 765 which is valid for the speeds we are interested in. We also assume that $\dot{\theta}$ is approximately constant,
 766 or $\dot{\theta} \approx 0$. By inspection of (A.2) $\dot{\theta}$ depends on θ but this is small, $\theta < \lambda/2$, for the steplengths under
 767 consideration. $\dot{\theta}$ also depends on $(\dot{\delta}\theta)$. While $\dot{\theta} \sim \Omega_0 < 1$, on an average $\dot{\delta}$ is close to zero suggesting
 768 a small effect coming from this term $(\dot{\delta}\theta)$. We shall see, that these approximations provide valuable
 769 qualitative and quantitative insights into the dynamics and the relationship between various relevant
 770 dynamical parameters.

771 B.2 Transition to double stance

As argued in the main manuscript, synchronization between the radial and angular motion relates γ and Ω_0 as

$$\Omega_0 = \left(\frac{\theta_\star}{\phi_\star} \right) \sqrt{\gamma},\tag{B.2}$$

where \star marks the values at the transition point between the single and double stance phases. From geometry, we can find θ_\star as

$$\sin \theta_\star = \frac{\lambda^2 + (1 - \delta_\star)^2 - 1}{2(1 - \delta_\star)\lambda}\tag{B.3}$$

while substituting $\delta = \delta_\star$, and $\omega t = \phi_\star$ in (B.1) yields

$$\cos \phi_\star = - \left(\frac{\gamma\delta_\star - 1}{1 - \gamma\delta_0} \right).\tag{B.4}$$

The dependence of θ_\star, ϕ_\star as a function of δ_\star are plotted in Figure 4B. In principle, the transition time can be found by solving

$$\lambda^2 + [1 - \delta(t_\star)]^2 - 2[1 - \delta(t_\star)]\lambda \sin \theta(t_\star) = 1.\tag{B.5}$$

772 so that $t_\star = t_\star(\lambda, \Omega_0, \gamma, \delta_0)$. One can then evaluate $\theta_\star = \theta(t_\star)$, and $\delta_\star = \delta(t_\star)$, to obtain the position
 773 of CoM at the transition, as well as the phase angle, $\phi_\star = \omega t_\star$. Thus all these quantities can be
 774 thought of as functions of four gait parameters, $\lambda, \Omega_0, \gamma$, and δ_0 .

775 B.3 Double stance phase

To approximate the double stance phase we are going to assume that the horizontal velocity and the vertical acceleration remain approximately constant. The intuition behind these approximations is as follows: the two springy legs provide horizontal forces in opposing directions so that we expect the average horizontal acceleration to be small and therefore the horizontal velocity to remain approximately constant. Realistic walking trajectories typically exhibit low-velocity changes which further strengthens this argument, and we compute the horizontal velocity at the start of the double stance. In contrast with the horizontal motion where the legs oppose each other, both legs provide a vertically upward forces. At the beginning of the double stance phase, all the force comes from the leg that was supporting the single stance phase at the touchdown, the swing leg is at its natural length. Thereafter, while the initial stance leg unloads, the leg that touched down loads. Therefore we conjectured that the net upward force may not change much, and approximate the net force as a constant. The approximate trajectories in the double stance phase are thus given by

$$\begin{aligned} x(t) &= (1 - \delta_*) \cos \theta_* + v_{x*}(t - t_*) , \\ y(t) &= (1 - \delta_*) \sin \theta_* + v_{y*}(t - t_*) + \frac{1}{2}a_{y*}(t - t_*)^2 . \end{aligned} \quad (\text{B.6})$$

where v_{x*} , v_{y*} , and a_{y*} can be calculated at the transition time as follows:

$$\begin{aligned} v_{x*} &= (1 - \delta_*)\Omega_0 \cos \theta_* , \\ v_{y*} &= -(1 - \delta_*)\Omega_0 \sin \theta_* , \\ a_{y*} &= F_{y*} = \gamma\delta_* \cos \theta_* - 1 . \end{aligned} \quad (\text{B.7})$$

776 The ultimate test of these approximations, of course, will obviously be provided by comparing it
777 with results from numerical simulation.

778 To summarize, Eqs. (2.5, B.5, B.6, B.7) together completely specifies a walking trajectory as
779 a function of $\lambda, \Omega_0, \gamma$, and δ_0 . We are now going to see how to maintain a steady limit cycle
780 gait these four parameters must obey a specific relationship that can be derived by looking at the
781 synchronization of the periodic angular and radial motion. We will also see how different gait
782 patterns emerge.

783 C Limit cycles

784 C.1 Constraint from periodicity and synchronization

785 A key requirement of a sustainable walking gait is that after a given step the CoM returns to the
786 same vertical height as the beginning of the cycle and also has the same velocity. Technically, the
787 gait cycle should be a limit cycle. This is a technical way of ensuring that the different types of
788 motion an animal undergoes are periodic and synchronized. For instance, in the context of the CoM
789 motion, the vertical and horizontal motion have to be synchronized and this imposes important
790 relationships between the parameters governing the dynamics, as we shall now see.

We will be able to derive this relationship by imposing that the time to reach the appropriate vertical and horizontal mid-step configuration that can be computed separately from the vertical and horizontal motion respectively, must be the same. For a limit cycle Using (B.6) we can calculate half of the horizontal distance traveled during the double stance:

$$x_d = \lambda/2 - (1 - \delta_*) \sin \theta_* , \quad (\text{C.1})$$

So, the half-time of the double stance phase is

$$\frac{1}{2}\tau_d = \frac{x_d}{v_x} = \frac{\lambda/2 - (1 - \delta_*) \sin \theta_*}{(1 - \delta_*)\Omega_* \cos \theta_*} , \quad (\text{C.2})$$

Now, due to the symmetry assumption, the vertical velocity is zero in the middle of the double stance phase. Therefore, it is possible to calculate t_d from the vertical kinematics as well

$$\frac{1}{2}\tau_d = \frac{\Delta v_y}{a_y} = \frac{0 - v_y}{a_y} = \frac{(1 - \delta_*)\Omega_* \sin \theta_*}{\gamma \delta_* \cos \theta_* - 1}, \quad (\text{C.3})$$

Therefore, from (C.2) and (C.3) we can conclude

$$\Omega_*^2 = \frac{(\gamma \delta_* \cos \theta_* - 1)(\lambda/2 - (1 - \delta_*) \sin \theta_*)}{(1 - \delta_*)^2 \sin \theta_* \cos \theta_*}, \quad (\text{C.4})$$

Since we suppose that the angular velocity is approximately constant during the single stance phase, we can rewrite it as

$$\Omega_0^2 = \frac{(\gamma \delta_* \cos \theta_* - 1)(\lambda/2 - (1 - \delta_*) \sin \theta_*)}{(1 - \delta_*)^2 \sin \theta_* \cos \theta_*} \equiv G_D(\delta_0, \delta_*, \gamma, \lambda), \quad (\text{C.5})$$

Moreover, from (2.9) we have

$$\Omega_0^2 = \left(\frac{\theta_*}{\phi_*}\right)^2 \gamma \equiv G_S(\delta_0, \delta_*, \gamma, \lambda). \quad (\text{C.6})$$

Thus, in order to have a synchronized limit cycle the four parameters, $\delta_0, \delta_*, \gamma, \lambda$ must be related:

$$G_D(\delta_0, \delta_*, \gamma, \lambda) = G_S(\delta_0, \delta_*, \gamma, \lambda). \quad (\text{C.7})$$

791 This explicitly demonstrates why all limit cycles can be characterized by only three parameters, for
792 instance by $\delta_0, \gamma, \lambda$, as Ω_0 and δ_* can be obtained via (C.6) and (C.7).

793 C.2 Different oscillatory mode solutions arise from the single stance phase 794 constraint

795 In this subsection we will see how the gait parameter space of periodic (limit cycle) walking separates
796 into different regions with different characteristic features. The different gaits fundamentally arise
797 because $\delta(t)$ is a periodic function. Technically, one can see its effect in the multivalued nature of
798 ϕ_* as a function of γ, δ_0 and δ_* as inferred from (B.4) using the cosine inverse. This in turn makes
799 G_S a multivalued function and choosing different branches while solving (C.7) leads to different
800 oscillatory limit cycle gaits. To understand this more intuitively suppose one wants to travel at a
801 given speed (approximately fixing Ω_0) and a given step-length (λ). What the oscillatory evolution
802 of $\delta(t)$ suggests is that even if one fixes the mid-stance contraction (δ_0), there may be more than
803 one way to achieve synchronization needed for limit cycle walking. For instance consider the single
804 stance synchronization condition (C.6): One can maintain approximately the same Ω_0 , with the same
805 transition angle ³, θ_* , either by choosing a relatively lower value of γ and oscillating less (smaller
806 ϕ_*), or have a much higher γ and oscillate more (ϕ_* approximately larger by a multiple of 2π). To
807 ensure that the upward velocity can be reversed during the double stance phase, the trajectory with
808 the smaller γ does require a little longer double stance time as compared to the larger γ trajectory.
809 So, the transition must occur a little earlier in the lower oscillatory mode, and accordingly t_*, δ_* , and
810 θ_* , are not exactly the same for the two trajectories. However, the flexibility of undergoing different
811 phases of oscillation approximately separated by multiples of 2π explains how the gait parameter
812 space separates into different oscillatory gaits, and why even with the same λ, Ω_0 and δ_0 , different
813 γ and correspondingly different oscillatory modes are possible.

³In other words, achieve approximately the same contraction length, δ_* , approximately at the same time, t_* .

814 D Approximate speed range for different oscillatory gaits

815 In this section, we provide a technical discussion on why the different oscillatory gaits are associated
816 with different speed ranges. We specifically demonstrate why it is not possible to walk too fast in
817 the normal walking gait.

818 D.1 Inverted and grounded running can lead to high walking-speeds.

We will first discuss the inverted walking gait whose CoM trajectory resembles that of the normal walking gait but has a different vGRF profile. We will show that while it is subjected to a lower bound in speed, one can theoretically walk much faster using this gait as compared to the normal walking gait. To see this, let us remind ourselves that for inverted walking approximately we have, $0 < \phi_\star < \frac{\pi}{2}$. According to (C.6), for a fixed γ one can decrease the speed by increasing ϕ_\star , but since the latter has an upperbound leading we have

$$\Omega_{0,\min}^2 = \left(\frac{2\theta_\star}{\pi}\right)^2 \gamma, \quad (\text{D.1})$$

819 where approximately θ_\star should be calculated by substituting $\delta_\star = \delta_{eq} = 1/\gamma$ consistent with $\phi_\star =$
820 $\pi/2$. Incidentally, this coincides with the upperbound for normal walking, see also Fig.?. In contrast
821 to having a lower bound in speed for a fixed γ , by decreasing ϕ_\star all the way to zero, the speed
822 can be increased arbitrarily according to the single stance constraint (C.6). Just as in the normal
823 walking gait though, the velocity redirection constraint coming from double stance phase limits the
824 maximum speed attainable and this bound agrees well with our numerical simulation. Nevertheless,
825 ϕ_\star can be much smaller in the inverted walking gait in comparison with the range available for
826 normal walking gait, and therefore much larger speeds can be accessed in this gait as compared to
827 the normal walking gait.

828 Let us next focus on the grounded running gait. In contrast to all other gaits the grounded
829 running gait has an inverted CoM trajectory where in between the mid-stance and mid-step during
830 the single stance phase, the CoM has a vertically upward velocity. This obviates the need to have
831 an upward force during the double stance phase in order to redirect the velocity. This means that
832 we should no longer require $\delta_\star > \delta_{eq} = 1/\gamma$. So, ϕ_\star need not satisfy, $0 < \phi_\star < \frac{\pi}{2}$, but could be
833 larger, as borne out by our simulations. More importantly, it is clear that in the grounded running
834 gait, the radial velocity can no longer be ignored as compared to the angular velocity, in fact, the
835 upward component of the radial velocity dominates over the downward component associated with
836 the angular motion. Thus our estimate of the transition velocity (B.7), which was essentially based
837 on angular motion, can no longer be trusted, and the limit cycle constraint (C.7) which gave rise
838 to the maximum speed-bound in other gaits, is no longer valid. Surprisingly though our analytical
839 estimates for such gaits continue to be broadly consistent with the numerical simulations, see Fig.?.
840 Intuitively, high speeds in normal walking gait became impossible to attain because the upward
841 force had a maximum and the time it had in the double stance phase shrunk with increasing speed
842 eventually making it impossible to redirect the vertical velocity. Grounded running is this very
843 special gait where the velocity in the single stance phase after the mid-step is upward and hence
844 there is no need for velocity redirection. Thus the speed maximum constraint coming from velocity
845 redirection is not applicable, and indeed in our numerical simulations we see the grounded running
846 gait to be able to access larger and larger speeds by increasing γ .

847 D.2 Normal walking is bounded by the double stance phase constraint

848 For normal walking we have shown that $\frac{\pi}{2} < \phi_\star < \frac{3\pi}{2}$. Moreover, we know that by varying δ_\star ,
849 θ_\star does not change too much (see Figure 4B). So according to (C.6), again we have two options

850 to increase the speed. Decreasing ϕ_* and increasing γ . However, in contrast to grounded running,
851 there is a conflict between these two options for normal walking. In summary, for high speeds, if ϕ_*
852 decreases as much as possible, we have $\phi_* \rightarrow \frac{\pi}{2}$, that leads to $\gamma\delta_* \rightarrow 1$; so the force might not
853 be enough to redirect the CoM velocity during double stance phase. In other words, the increase in
854 speed needs an increase in transition force; and to have the maximum transition force we must have
855 $\gamma\delta_* \rightarrow 2$, which leads to $\phi_* \rightarrow \pi$. So at the upper bound of speed, to satisfy both constraints
856 from single and double support phases ((C.5) and (C.6)), ϕ_* settles somewhere between $\frac{\pi}{2}$ and π .
857 On the other hand, there is only a little effect of the double stance constraint on the lower bound
858 of speed (see Figure 5G and S??). This boundary deviation from the single stance constraint can
859 be observed better for high values of γ in which the need for higher force increases. For the lower
860 bound, although ϕ_* is somewhere between $\frac{3\pi}{2}$ and π , it is much closer to $\frac{3\pi}{2}$ rather than π .

861 **D.3 Slow walking via multiple oscillation modes**

862 According to (C.6), by increasing ϕ_* over the normal walking range, it is quite possible to jump to the
863 slow walking region. In this situation, since there is no concern about the speed-force relationship,
864 the double stance constraint does not play the main role again.

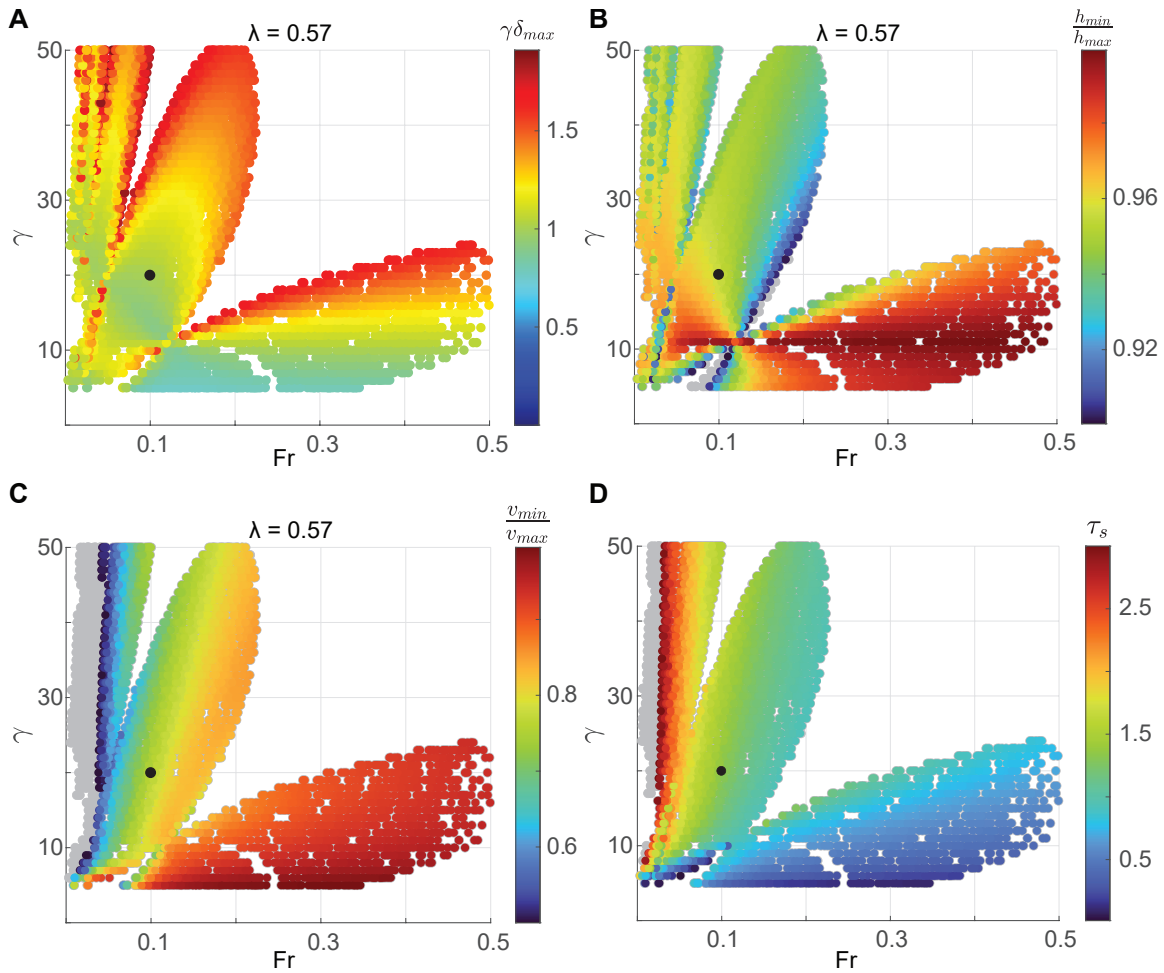


Figure S1. How important dynamic and kinematical features vary across gaits. **A.** We show how the maximal force, $\gamma\delta_{\max}$, exerted during a gait cycle varies across limit cycles. We note that lower the number of oscillations the lower is the maximal force required. In **B.** and **C.** We assess how the height and horizontal speed varies during a gait cycle by calculating the ratio between their maximum and minimum values, h_{\min}/h_{\max} , and v_{\min}/v_{\max} respectively. We note that while the variations in the normal gait lies mostly within the ranges observed in humans, the higher oscillatory gaits show a larger variation in speed. **D.** Here we depict how the single-stance or swing time varies across different gait cycles. We see that cycles more number of oscillations have a longer time and therefore lower frequency. Since energy loss due to swing increases with higher frequency, this suggests that high oscillatory modes are energetically preferred. In all these figures the black dot represents the limit cycle that best fits experimental walking data at 2 miles/hour. We note that it exhibits relatively small variation in speed and height. Moreover, as compared to inverted gait cycles (at the same speed) it expends less swing energy, and as compared to higher oscillatory modes exerts less force. In concert, these plots argue why the normal gait is the preferred gait.

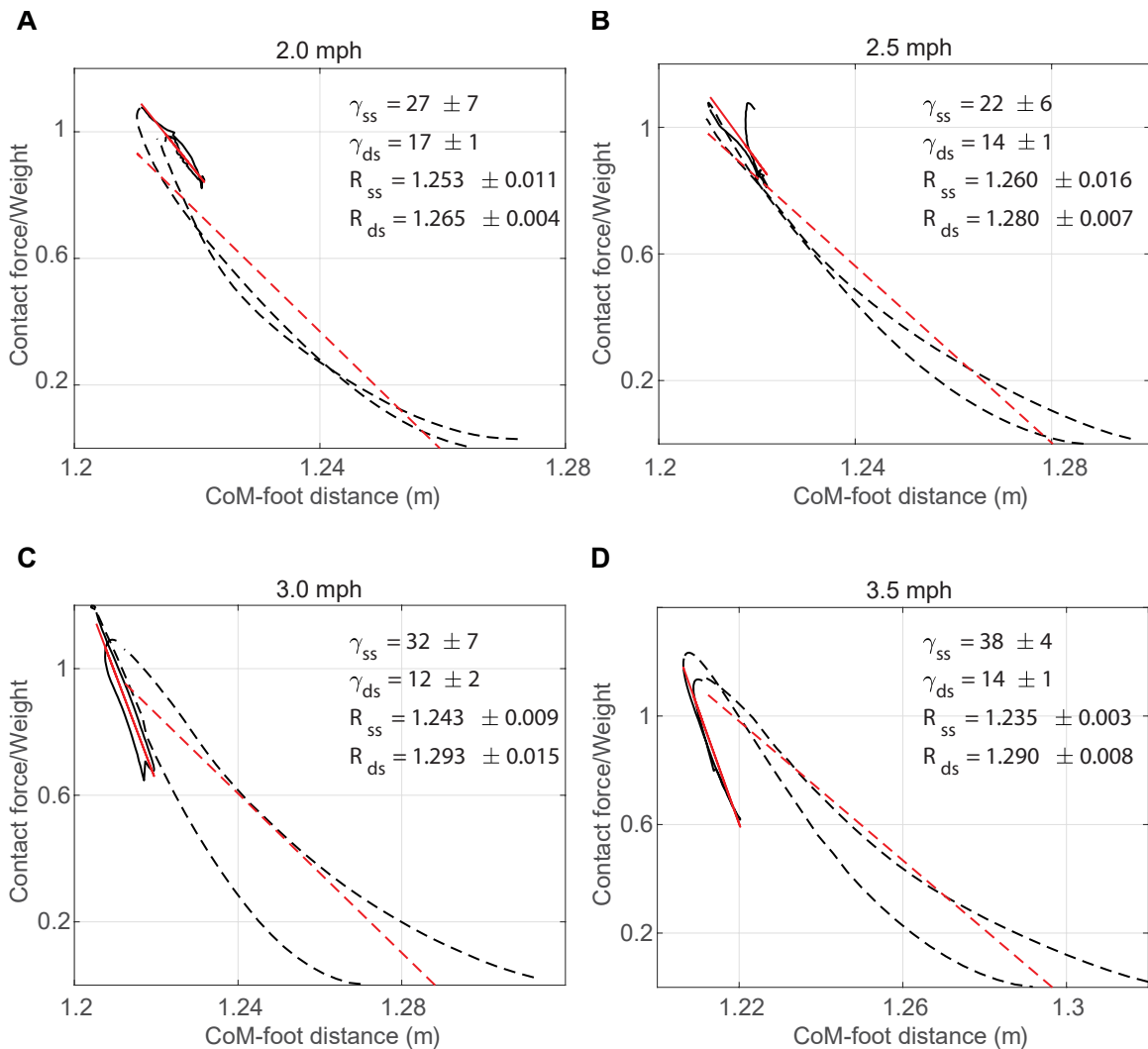


Figure S2. Force-length relationship shows that except for walking at 2.5 mph, the spring constants during single and double stance phases are different Each panel shows the force-length relationship for a single step. Dotted black line is during the single support phase, and solid black lines are during the double support phase. Red dotted and solid line show the best fitting linear spring to the single and double support phases. The mean and the SD of the spring constants and natural leg length are also reported for each speed.

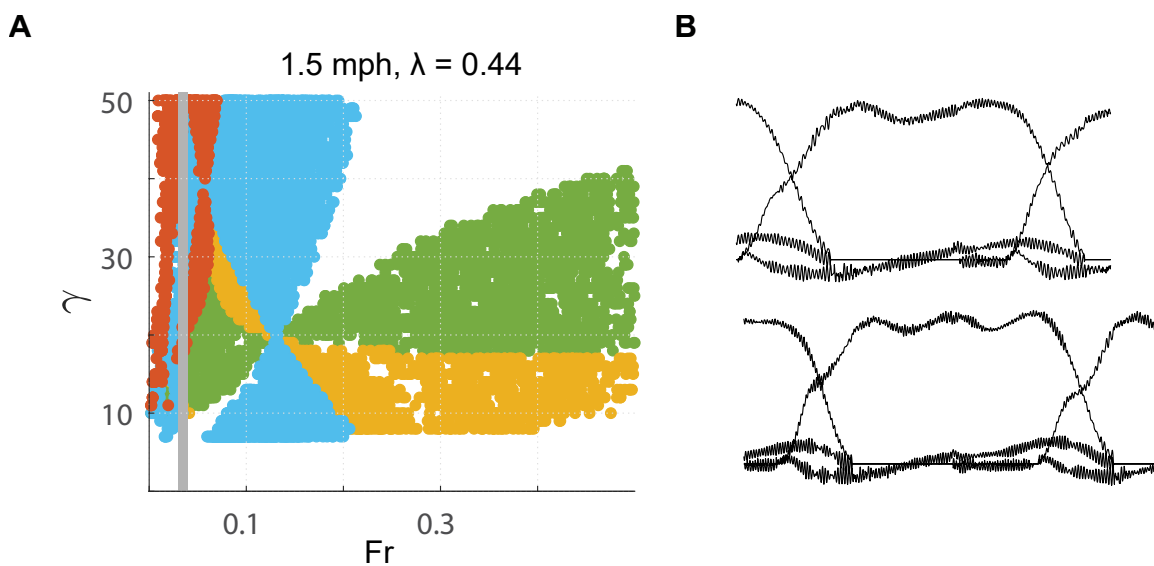


Figure S3. Human walking can involve higher oscillatory modes at low speed . A. At low speeds, such as, at a Fr number of 0.04 (gray line), both an M-shaped GRF (blue), and higher oscillation mode (orange) are possible. **B.** vGRF at these walking speeds can show both an M-shaped GRF, and GRF with higher number of oscillation as seen by the three-humped vGRF pattern.

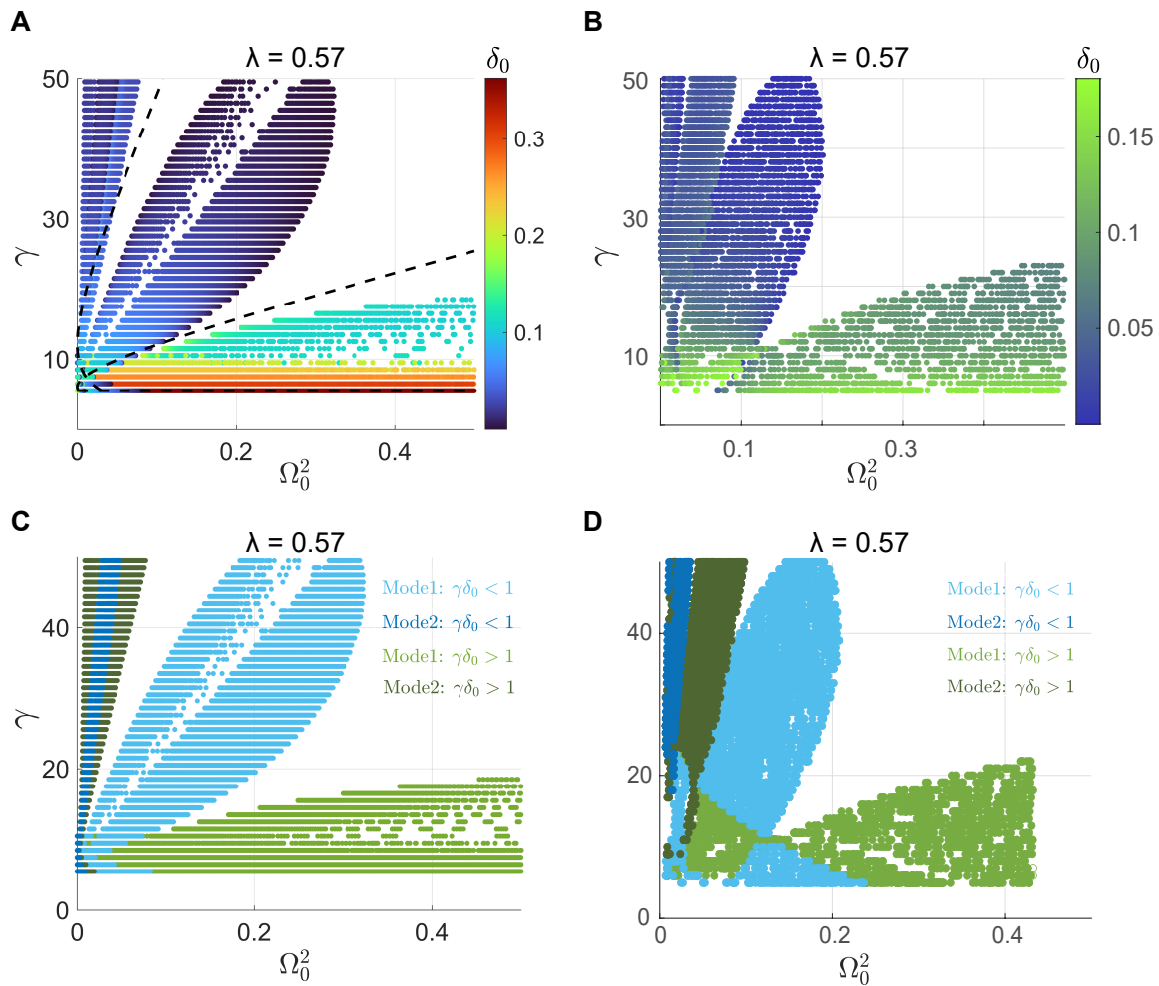


Figure S4. Comparison between analytically and numerically obtained limit cycles. **A.** We show the analytical solutions for a fixed step-length that are characterized by three quantities: the x-axis and y-axis corresponds to Ω_0^2 and γ respectively, while the color represents the value of δ_0 . **B.** To compare with the analytical results we here depict numerical limit cycle solutions using the same color axis scale to represent δ_0 values. The analytical and numerical plots show similar patterns, and while the analytical solution over-estimates the value of δ_0 , its variation both along the Ω_0^2 -axis and γ -axis show similar trend as the numerical plot. **C.** and **D.** shows the same plots as **A.** and **B.** respectively, except that the color now represents the identity of the gait, normal, inverted or exhibiting multiple oscillations. While there are some discrepancies between the analytical and numerical results, they are broadly consistent with each other.